ORNL-TM-4847
(ENDF-218)

Cross Section and Method Uncertainties: the Application of Sensitivity Analysis to Study Their Relationship in Radiation Transport Benchmark Problems

C. R. Weisbin
E. M. Oblow
J. Ching
J. E. White
R. Q. Wright
J. Drischler

OAK RIDGE NATIONAL LABORATORY
OPERATED BY UNION CARBIDE CORPORATION • FOR THE U.S. ATOMIC ENERGY COMMISSION

ORNL-TM-4847
(ENDF-218)

Contract No. W-7405-eng-26

Neutron Physics Division

CROSS SECTION AND METHOD UNCERTAINTIES: THE APPLICATION OF SENSITIVITY ANALYSIS TO STUDY THEIR RELATIONSHIP IN RADIATION TRANSPORT BENCHMARK PROBLEMS

C. R. Weisbin, E. M. Oblow, J. Ching,* J. E. White,
R. Q. Wright, and J. Drischler

*Present address: Energy, Inc., Idaho Falls, Idaho.

NOTE:

This Work Partially Supported by
DEFENSE NUCLEAR AGENCY
Under Subtask PC104
and the
U.S. ENERGY RESEARCH AND DEVELOPMENT ADMINISTRATION

AUGUST 1975

OAK RIDGE NATIONAL LABORATORY
Oak Ridge, Tennessee 37830
operated by
UNION CARBIDE CORPORATION
for the
ENERGY RESEARCH DEVELOPMENT ADMINISTRATION

TABLE OF CONTENTS

ABSTRACT

Sensitivity analysis is applied to the study of an air transport benchmark calculation to quantify and distinguish between cross-section and method uncertainties. The boundary detector response was converged with respect to spatial and angular mesh size, P_ℓ expansion of the scattering kernel, and the number and location of energy grid boundaries. The uncertainty in the detector response due to uncertainties in nuclear data is 17.0% (one standard deviation, not including uncertainties in energy and angular distribution) based upon the ENDF/B-IV "error files" including correlations in energy and reaction type. Differences of approximately 6% can be attributed exclusively to differences in processing multigroup transfer matrices. Formal documentation of the PUFF computer program for the generation of multigroup covariance matrices is presented.

I. INTRODUCTION

The complete ORNL cross-section sensitivity and uncertainty analysis system (FORSS)[1] has been applied to estimate the overall uncertainty and the contribution of individual components in several calculational benchmark transport problems. Only relatively simplified geometries were considered so that uncertainties due to spatial modelling were considerably reduced. Since the availability of evaluated uncertainties and their correlations in energy and reaction type is limited in ENDF/B-IV but do exist for N and O, this report describes the analysis of an air transport benchmark problem including the estimation of the effects of uncertainties in nuclear data. It also includes a detailed description of the PUFF computer program which was used to generate multigroup covariance files.

Cross-section sensitivity studies of radiation transport in air have been underway for several years. The most recent and complete analysis is that of Bartine et al.,[2] which includes preliminary estimates of the uncertainty in cross section over broad energy ranges based on simplified assumptions about data correlations. The present work extends this type of analysis by incorporating the final, and very detailed, ENDF/B-IV uncertainty files including covariance as a function of energy and reaction type. It then attempts to go further by quantifying other types of uncertainties introduced in the analysis procedure.

Section II presents the problem characteristics pointing out the differences between the specifications used in ref. 2 and those for the present study. Section III describes the sensitivity methodology[2,3] used in conjunction with the point-energy discrete-ordinates technique[4] to attempt to converge[5] the results with respect to the energy grid used. Section IV reviews the formulation for processing large multigroup covariance matrices[6] with spatial emphasis placed on display techniques and bulk data management schemes. Differences due to divergent cross-section processing techniques[7] are treated, in Section V, by successive runs with different processed sets and with projections based upon sensitiv-

ity theory. Section VI presents the results of folding covariance matrices with sensitivity profiles to estimate uncertainties due to nuclear data. The effects of using different transport methods are assessed only briefly in Section VII by comparing the results from Discrete Ordinates and Moments Method techniques. Section VIII summarizes the results and conclusions of the entire study.

II. BENCHMARK PROBLEM DEFINITION

The source geometry approximates a point source at the center of a sphere of air of radius r_o. A uniformly distributed, isotropic source is contained within a region, characterized by radius r_s, sufficiently small with respect to the dimension of the transport media, r_o. A detector with a flat energy response $\Sigma_D = 1.0\ cm^{-1}$, is distributed in a zone from r_D to r_o. The geometry is shown in Fig. 1.

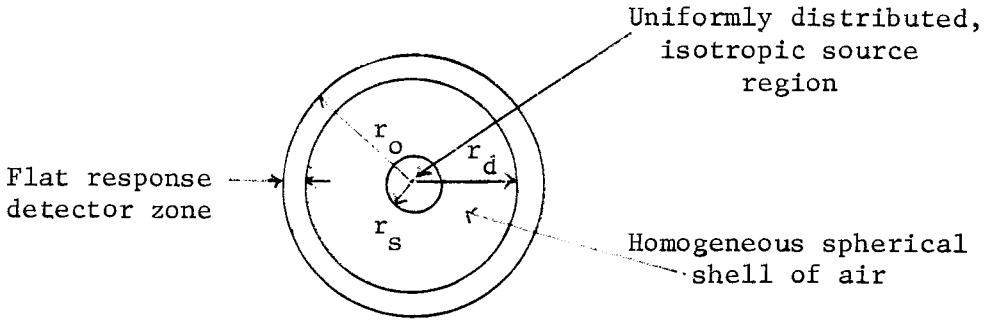

Fig. 1. Geometric Model Employed

$r_d = 1990$ m

$r_s = 12.5$ m

$r_o = 2000$ m

$\rho_{^{14}N} = 4.25 \times 10^{-5}$ (atoms/barn-cm)

$\rho_{^{16}O} = 1.13 \times 10^{-5}$ (atoms/barn-cm)

In order to standardize the source description in a form which is both general for fission and fusion devices and useful for recalculation with other methods and group structures, an analytic representation was chosen. The source spectrum was obtained by superposition of a Gaussian energy distribution around 14 MeV and a Watt fission spectrum peaked around 1 MeV. More precisely, the source spectrum was represented analytically in terms of a Gaussian

$$G(E) = G_o \, e^{-\frac{1}{2}[(E-E_o)/(\Delta E)]^2} \tag{1}$$

and a Watt fission spectrum

$$F(E) = F_o \, e^{-E/\alpha} \sinh[(\beta E)^{\frac{1}{2}}] \tag{2}$$

where E is the neutron energy in MeV, E_o = 14 MeV, ΔE = 1 MeV, α = 1 MeV, β = 2 MeV^{-1}, G(E) and F(E) are in units of source neutrons/sec-MeV-cm^3, and the constants G_o and F_o are determined by normalizing the total source strength to unity over the energy range of interest with half of the neutrons coming from each of the distributions. That is

$$\int_E \int_{r_s} G(E) \, dE \, dV = \int_E \int_{r_s} F(E) \, dE \, dV = 0.5 \quad . \tag{3}$$

A graph of the source spectrum is presented in Fig. 2. The transport characteristics of the media are illustrated in Fig. 3 which presents the macroscopic total cross section for air between 100 keV and 15 MeV. The quantity of interest is the flux everywhere in the system and, in particular, the response of a flat detector of unit cross section in the zone at 2000 meters.

The problem specifications presented above differ significantly in several important respects from the problem analyzed in ref. 2. In the earlier work, the quantity of interest was the total (neutron and gamma ray) tissue dose at 2000 meters from a prototypical thermonuclear source. This work focuses primarily on total integrated boundary flux (i.e., the

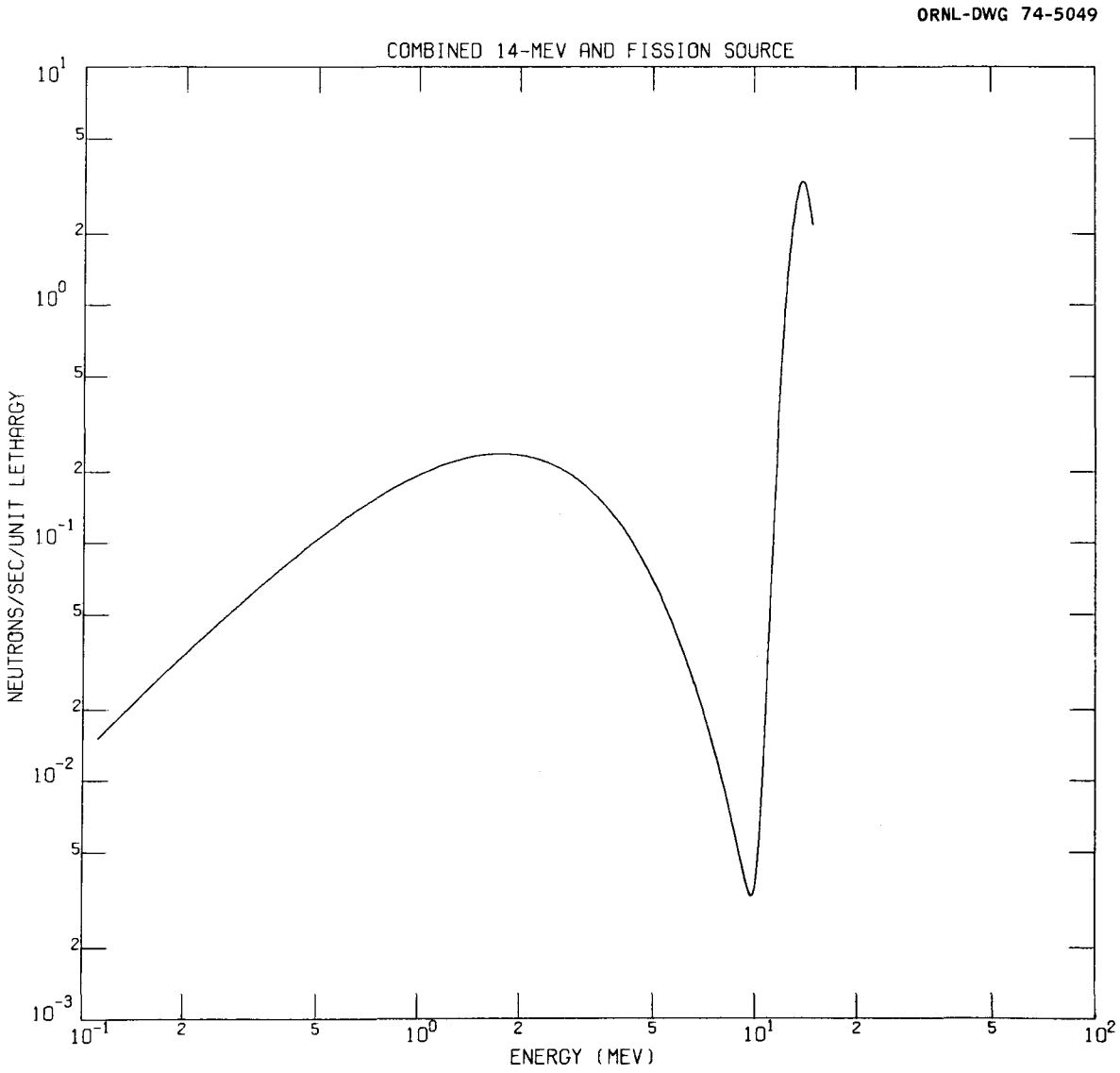

Fig. 2. Air Transport Benchmark Source Spectrum.

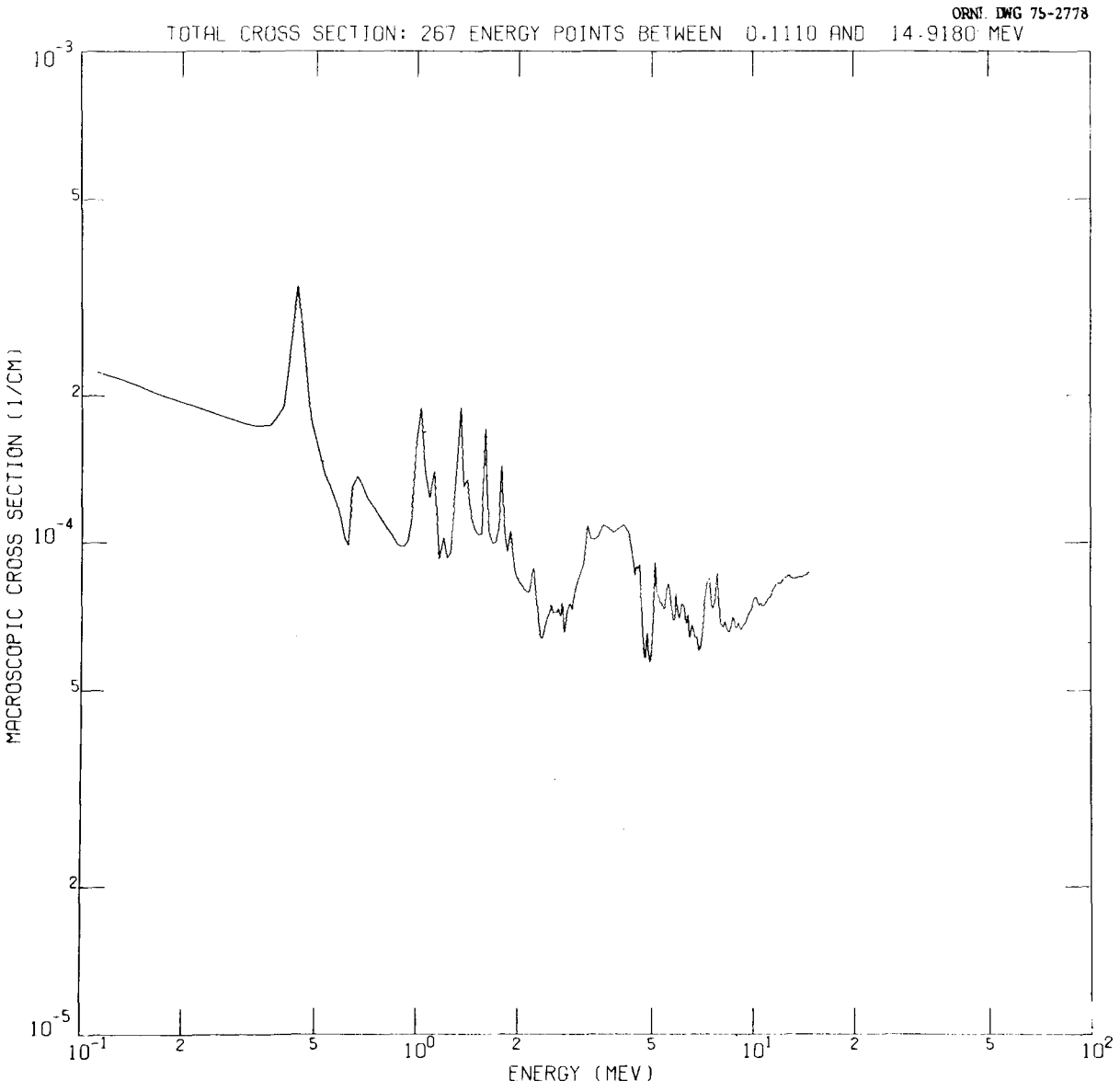

Fig. 3. Macroscopic Total Cross Section for Air Between 100 keV and 15 MeV.

response of the flat detector) arising from a hypothetical 14-MeV Gaussian source with an equal fission component. The number densities in ref. 2 were 3.664×10^{-5} for N and 9.74×10^{-6} for O, markedly different from those taken for this work and presented in Fig. 1. Finally, the problem was solved earlier in a 101-33 coupled neutron and gamma-ray energy group structure, using ENDF/B-III MAT 1133, Mod 3 for ^{14}N and MAT 1134, Mod 1 for ^{16}O. This work finalized on a 266-group optimized structure, selected using MAT 4133 Mod 3 and MAT 4134 Mod 1 while the complete uncertainty analysis using this multigroup structure was based on cross-section sets from ENDF/B-IV, MAT 1275 for ^{14}N and MAT 1276 for ^{16}O. For completeness, an uncertainty analysis on the specific problem defined in ref. 2 is included in Appendix A.

III. ENERGY GRID SELECTION AND CONVERGED SOLUTIONS

The key element in the creation of a fine-energy structure solution to the benchmark problem was the selection of a fine-structure energy grid. The point-energy processing code MOMANS[4] and a point-energy version of the SWANLAKE[8] sensitivity code was used for this purpose. The great speed and flexibility in generating processed neutron cross sections and sensitivity results on a pointwise energy grid make it possible to converge transport results as a function of the number and location of energy boundaries.

The convergence procedure is described as follows. First, an integral flux parameter was chosen for the problem defined in Section II ; the result of interest was the total boundary detector response. The response at the outer boundary in a shielding situation was found to usually ensure equal or better convergence of the total flux versus distance throughout the rest of the shield system. Next, a fine point-energy solution of the benchmark problem was obtained using a point energy grid. These results were then analyzed with the point-energy sensitivity code to select an initial few-point energy grid ($\sim$40 points) to begin convergence tests. This initial grid was chosen by constructing a cumulative probability function for the sensitivity profile as a function of energy and then selecting energy boundaries invoking an equal total importance criteria.[5] That is, the group boundaries are selected so that the reaction rates, biased by an importance function, is divided equally among the

energy groups. In the terminology of sensitivity theory, each energy group is chosen to be equally sensitive in absolute magnitude to all the multigroup cross-section data. Hence, any error introduced in subsequent approximations of the weighting flux in the multigroup averaging process would be spread more uniformly over the entire energy range. This initial grid is not equally spaced in lethargy as was the starting grid.

The second phase of the benchmark calculation consisted of convergence tests to ensure high accuracy of the final flux results within the limitations of computer storage and run time. Thus, the few point grid (41 points) was used as energy boundaries and successive multigroup runs were made with ANISN[9] to attempt to converge the solution with respect to spatial and angular mesh interval size and P_ℓ expansion of the scattering kernel. When 1% or better convergence was achieved on this scale, additional energy boundaries (in multiples of the number in the original few-point grid) were added uniformly and point discrete-ordinates calculations performed to try to converge the results in energy. This latter procedure was carried out until either 1% convergence was achieved or cross-section core storage requirements were exceeded. Finally, the optimized energy bounds were used as the multigroup structure for computation of forward and adjoint fluxes for use in the analysis presented in subsequent sections.

With the following notation:

P_ℓ - Legendre expansion of the scattering kernel

S_N - Discrete angles at which the angular flux is calculated

I_m - Spatial intervals used in problem solution

J_k - Number of energy groups employed for solution

E - Relative error given by

$$\frac{F\ (\text{run of interest}) - F\ (\text{best converged run})}{F\ (\text{best converged run})} \times 100$$

F - Boundary detector response (or mathematically)

$$\int_{111\ keV}^{15\ MeV} \int_{r_d}^{r_o} \phi_o(E,r)\ dE\ dV$$

and the initial problem parameters set as P_3, S_{16}, I_{82}, J_{40}. Tables I through IV indicate the type of convergence achieved.

Table I. P_ℓ Convergence for Legendre Expansion of Scattering Kernel

P_ℓ	P_1	P_2	P_3	P_5
F	2.490	2.760	2.774	2.772
E(%)	-10.17	-0.43	-0.07	0

Table II. S_N Convergence for Angular Flux Quadrature

S_N	S_8	S_{12}	S_{16}	S_{20}	S_{24}
F	2.503	2.714	2.774	2.831	2.861
E(%)	-12.51	-5.14	-3.04	-1.02	0

Table III. I_m Convergence for Spatial Intervals

I_m	I_{43}	I_{82}	I_{121}	I_{201}	I_{281}
F	2.557	2.774	2.855	2.900	2.910
E	-12.13	-4.67	-1.89	-0.34	0

Table IV. J_k Convergence for Number of Energy Groups (Number Points -1)

J_k	J_{40}	J_{78}	J_{116}	J_{154}	J_{192}	J_{166}
F	2.774	2.493	2.305	2.452	2.481	2.454
E	13.04	1.59	-6.07	-0.08	1.10	0

The final results of the convergence test indicated that good convergence of the response ($\leq$5%) could be achieved with the following parameter set: P_3, S_{24}, I_{201}, and J_{266}. The convergence of the final set of problem parameters was examined by reducing the specifications jointly (P_2, S_{20}, I_{121}, J_{192}) and observing the convergence to within 1%. Figures 4 and 5 illustrate the converged scalar flux spectrum at 2000 meters and the adjoint spectrum at the center of the sphere.

IV. PROCESSING UNCERTAINTY FILES

A. Formulation of Multigroup Covariance Matrices

Only recently have standard formats and procedures been established within the ENDF/B system[10] for the processing of evaluated and correlated energy-dependent uncertainty information into a multigroup covariance matrix formulation. These covariance matrices were established to permit systematic sensitivity investigations[11,12] to determine, in a credible fashion, what cross-section measurements, evaluation, or processing methods most need further refinement.

Some of the guiding principles behind the formulation of the uncertainty files for microscopic cross sections are designed to:

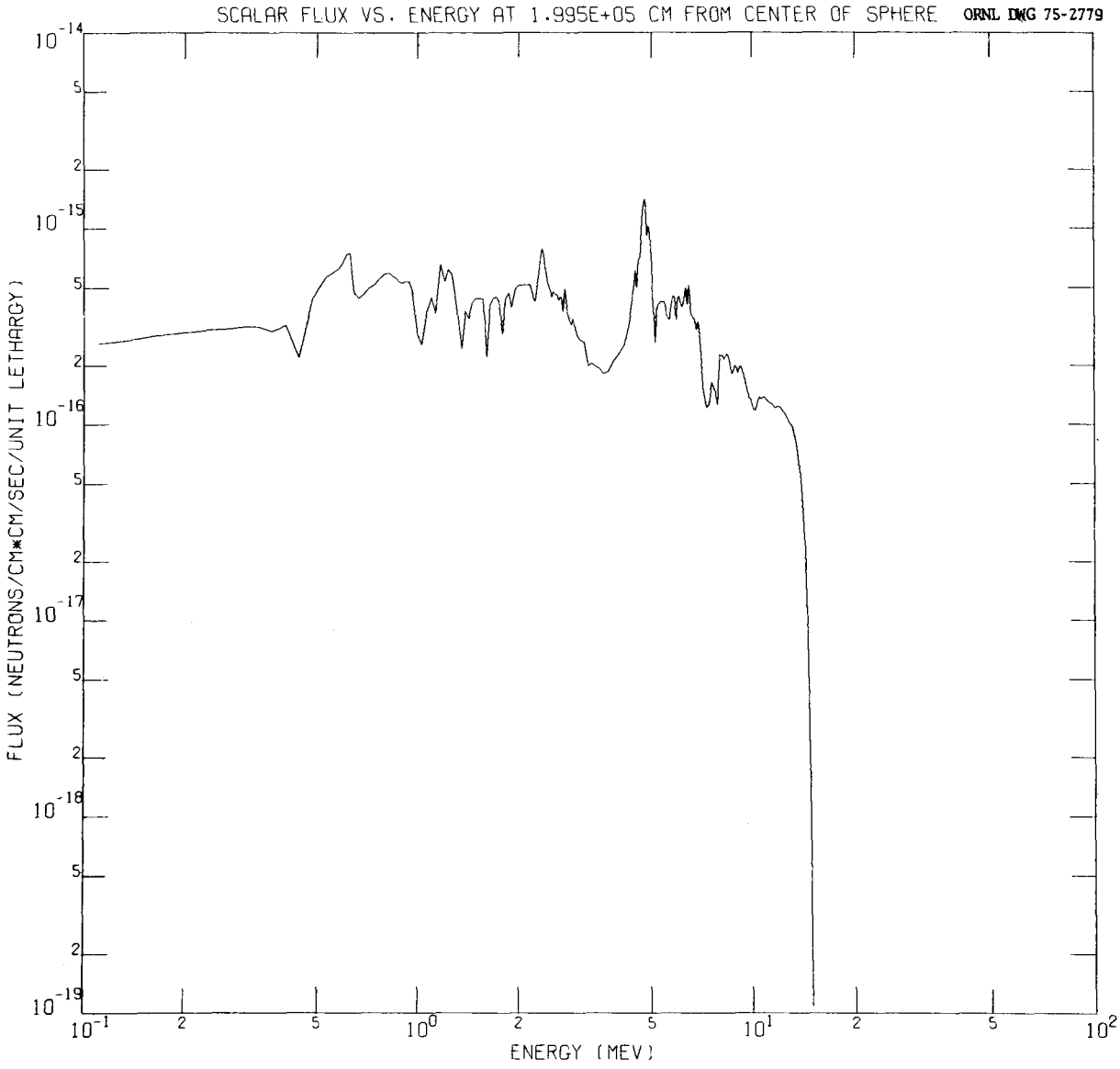

Fig. 4. Total Scalar Flux Spectrum at 2000 Meters - Air Transport Benchmark Problem.

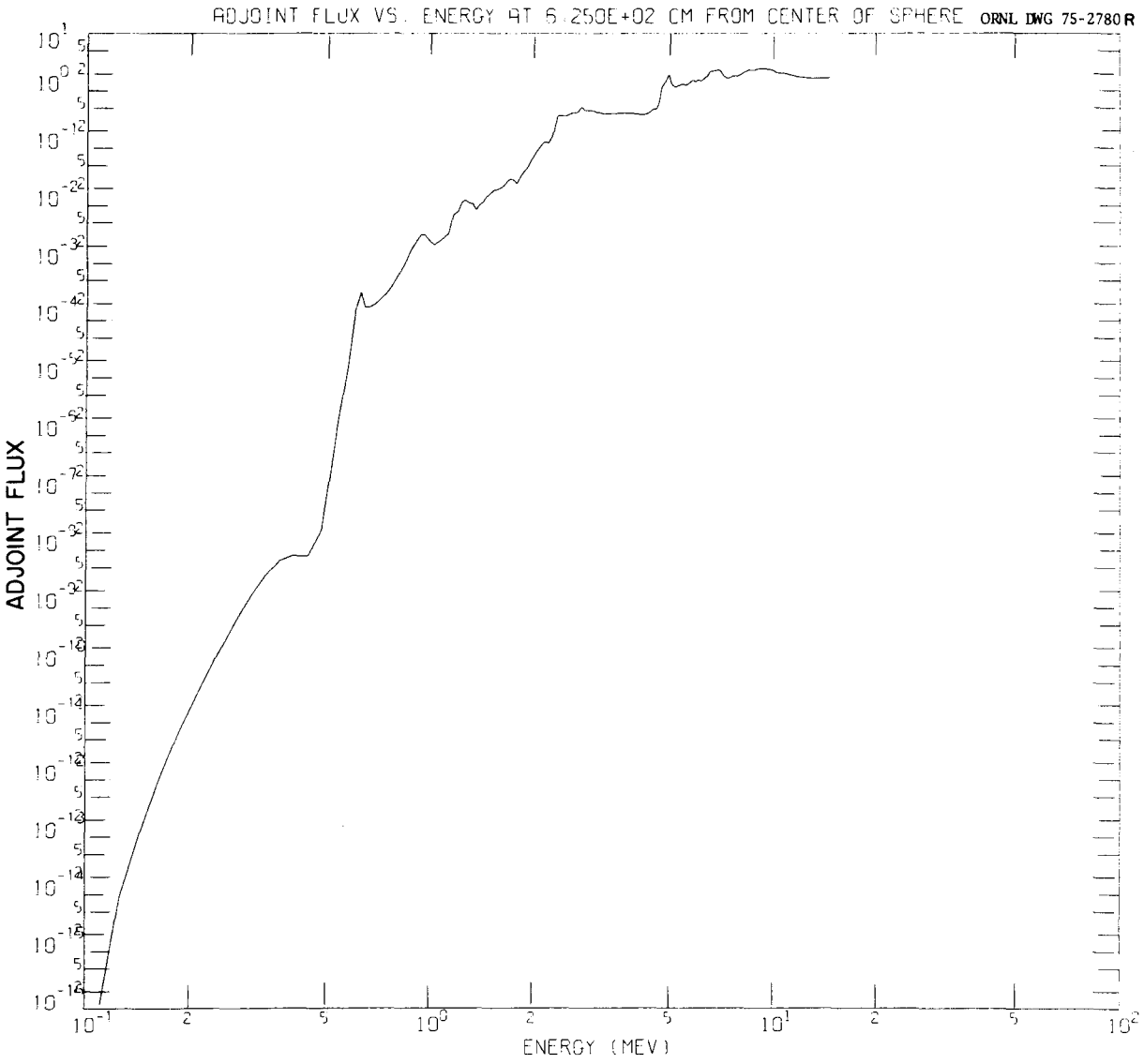

Fig. 5. Adjoint Spectrum at the Center of the Sphere - Air Transport Benchmark Problem.

1. Provide a unique format for the estimated uncertainties which is flexible, but not unwieldly.
2. Permit the information to be processed at the same time as the cross-section data without imposing an undue burden on cross-section processing codes.
3. Promote the use of the file by implementation of a format to which experimental uncertainties could be readily translated.

With this in mind, the types of covariance representations permitted[10] in ENDF/B-IV include:

LB=0 absolute components only correlated over each E_k interval

$$\mathrm{Cov}(X_i,Y_j) = \sum_k P^{i;k}_{j;k} F_{XY,k} \tag{4}$$

LB=1 fractional components only correlated over each E_k interval

$$\mathrm{Cov}(X_i,Y_j) = \sum_k P^{i;k}_{j;k} F_{XY,k} X_i Y_j \tag{5}$$

LB=2 fractional components correlated over all E_k intervals

$$\mathrm{Cov}(X_i,Y_j) = \sum_{k,k'} P^{i;k}_{j;k'} F_{XY,k} F_{XY,k'} X_i Y_j \tag{6}$$

LB=3 fractional components correlated between E_k and E_ℓ intervals

$$\mathrm{Cov}(X_i,Y_j) = \sum_{k,\ell} P^{i;k}_{j;\ell} F_{X,k} F_{Y,\ell} X_i Y_j \tag{7}$$

where X_i and Y_j represent cross sections X and Y evaluated at energies i and j, respectively, the F's ($F_{XY,k}$, $F_{XY,k'}$, $F_{X,k}$ and $F_{Y,\ell}$) represent uncertainty coefficients, taken directly from the ENDF/B file, describing the correlation between cross sections X and Y for a specific energy interval. These fractional components are defined with respect to assumed normal distribution of cross-section uncertainties; furthermore,

multiple sections (e.g., $F^{n}_{XY,k}$) may be provided to identify specific types of experimental uncertainties associated with the complete covariance matrix. The $F_{XY,k}$ and $F_{XY,k'}$ are taken from a single table of energy-dependent correlation information for reactions X and Y. The $F_{X,k}$ and $F_{Y,\ell}$ indicates that the covariance data for these reactions are taken from two independent tables, one for X and one for Y. The $P^{i,k}_{j,k'}$ is zero except for the case when energy i is contained within energy interval k and energy j is contained within energy interval k'. $Cov(X_i,Y_j)$ is then the covariance between cross section X and energy i and cross section Y at energy j. There is a fifth law (LB=4), but since it can be described as combinations of the first four, no data has yet been cast in this form for ENDF/B-IV.

This type of formulation (sums of quantities separable in X and Y) has the very desirable characteristic that if one assumes a flux model uncorrelated to the cross sections of interest, the multigroup covariance matrices are reduced to combinations of single integrals involving group fluxes and cross sections which can be calculated easily. In particular, for

LB=0,

$$Cov(X_G,Y_H) = \frac{\sum_n \sum_k F^n_{XY,k}\ \phi^n_{G,k}\ \phi^n_{H,k}}{\phi_G\ \phi_H} \tag{8}$$

LB=1,

$$Cov(X_G,Y_H) = \frac{\sum_n \sum_k F^n_{XY,k}\ \phi^n_{G,k}\ X^n_{G,k}\ \phi^n_{H,k}\ Y^n_{H,k}}{\phi_G\ \phi_H} \tag{9}$$

LB=2,

$$Cov(X_G,Y_H) = \frac{\sum_n \left(\sum_k F^n_{XY,k}\ \phi^n_{G,k}\ X^n_{G,k}\right)\left(\sum_{k'} F^n_{XY,k'}\ \phi^n_{H,k'}\ Y^n_{H,k'}\right)}{\phi_G\ \phi_H} \tag{10}$$

LB=3,

$$\mathrm{Cov}(X_G,Y_H) = \frac{\sum_n \left(\sum_k F^n_{X,k}\ \phi^n_{G,k}\ G^n_{X,k}\right)\left(\sum_{k'} F^n_{Y,k'}\ \phi^n_{H,k'}\ Y^n_{H,k'}\right)}{\phi_G\ \phi_H} \qquad (11)$$

The derivation of Eqs. (8-11) are fully described in ref. 10; the notation used here is:

$\mathrm{Cov}(X_G,Y_H)$ = Multigroup covariance between reaction X group G as it relates to reaction Y, group h.

ϕ_G = Multigroup flux per user group G.

$X^n_{G,k}$ = Multigroup cross section for reaction X for a super-group (G,k) constructed from the union of energy bounds for interval k (taken from subsection n) and those which were user input. $\phi^n_{G,k}$ is the flux for this group.

B. Implementation

The PUFF processing system[13] based on the MINX[14] multigroup processing code was developed specifically to read the ENDF/B-IV "error" files and construct multigroup covariance matrices according to Eqs. (8-11). For detailed programming considerations, the reader is referred to Appendix B of this report.

The salient features are noted below:

1. Multigroup cross sections and fluxes are computed for a group structure which is the union between the user group structure and all energies used in the error file description for all the reactions and materials of interest. This supergroup structure obviously can get very large quite rapidly as the size of the problem considered and the level of detail available in the files expand.

2. The large number of fluxes and cross sections required have been appropriately labelled for subsequent automated retrieval. (Note

that most processing codes normally do not preserve group flux values.)

3. All programming reflects variable dimensioning storage allocation.
4. All new coding is transparent to the MINX user not interested in processing error files. There is a single input flag which is 0/1; no error processing required/process errors. All other input is identical to a normal multigroup processing run. It should also be noted that with just a single additional input flag, the error processing input is quite user-oriented.

C. Results for Processed Uncertainty Files

Several quantities related to uncertainties in multigroup cross sections have been derived from the pointwise ENDF/B 'error' file. Clearly, of interest, is the covariance matrix

$$\mathrm{Cov}(X_G,Y_H) = \left\langle (X_G - \bar{X}_G)(Y_H - \bar{Y}_H) \right\rangle \tag{12}$$

for reaction X, group G as it relates to reaction Y, group H, and the associated quantity, the relative covariance matrix.

$$\mathrm{Rel\ Cov}(X_G,Y_H) = \mathrm{Cov}(X_G,Y_H)/X_G Y_H \tag{13}$$

In this notation, the standard deviation is given by:

$$\mathrm{Std.\ Dev}(X_G) = \sqrt{\mathrm{Cov}(X_G,X_G)} \tag{14}$$

and the analogous relative quantity, the relative standard deviation, is

$$\mathrm{Rel\ Std.\ Dev}(X_G) = \frac{\mathrm{Std.\ Dev}(X_G)}{X_G} \tag{15}$$

It is reasonable to expect that the covariance matrix of energy-dependent cross sections is strongly diagonal, i.e., the magnitude of the matrix elements tend to be small for groups G and H significantly displaced from each other in energy. However, the greater number of off-diagonal terms makes it difficult to say, a priori, that only the diagonal elements need be considered.

The correlation matrix is a quantity constructed by dividing the relative covariance matrix for X_G and Y_H by the respective relative standard deviations.

$$\mathrm{Corr}(X_G,Y_H) = \frac{\left\langle (X_G - \bar{X}_G)(Y_H - \bar{Y}_H) \right\rangle}{\sqrt{\left\langle (X_G - \bar{X}_G)^2 \right\rangle \left\langle (Y_H - \bar{Y}_H)^2 \right\rangle}} \tag{16}$$

The correlation matrix is bounded by unity, i.e.,

$$\left|\mathrm{Corr}(X_G,Y_H)\right| \leq 1 \tag{17}$$

When $\mathrm{Corr}(X_G,Y_H) = 0$, the group cross sections are said to be totally uncorrelated; when $\left|\mathrm{Corr}(X_G,Y_H)\right| = 1$, the group cross sections are termed fully correlated.

Figures 6 through 8 illustrate some of the processed correlation matrices and standard deviations obtained for nitrogen and oxygen. Appendix C of this report presents a complete set of correlation matrices (and standard deviations) for all energies and reaction types for N and O. These graphs are given in 22 groups for clarity of presentation. The actual matrices used in the section on results correspond to the problem described in this paper (266 groups). Figure 6 presents the correlation matrix for elastic scattering (reaction 2) as a function of energy as well as the standard deviation for ^{14}N. Several points are immediately noteworthy. First, the standard deviation has not appreciably changed from its description in ref. 2 (this is true for all reactions for N and O); the cross section is reasonably well known at lower energies ($\sim$3%)

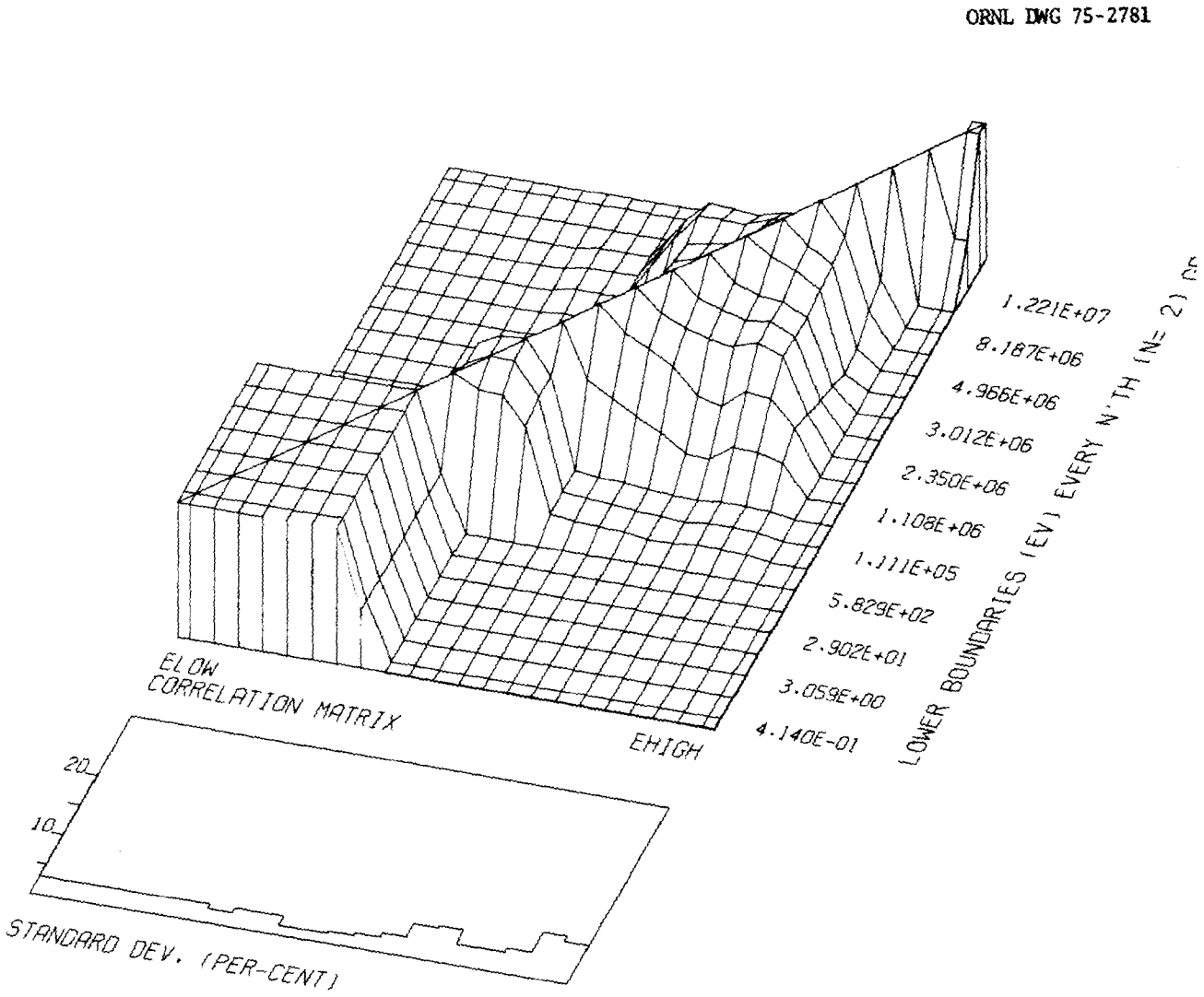

Fig. 6. Correlation Matrix and Standard Deviation for the ^{14}N Elastic Scattering Cross Section.

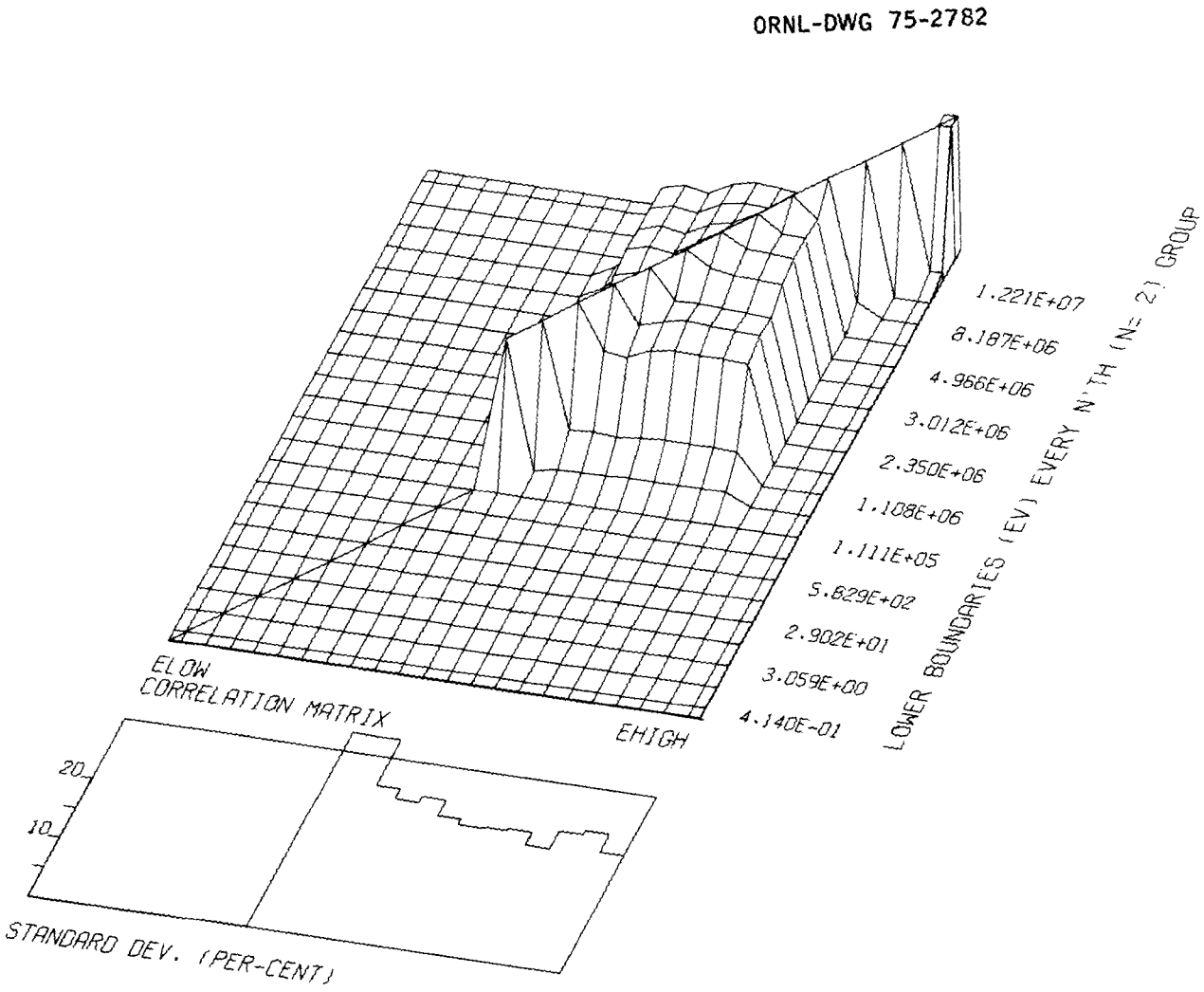

Fig. 7. Correlation Matrix and Standard Deviation for the $^{14}N(n,\alpha)$ Cross Section.

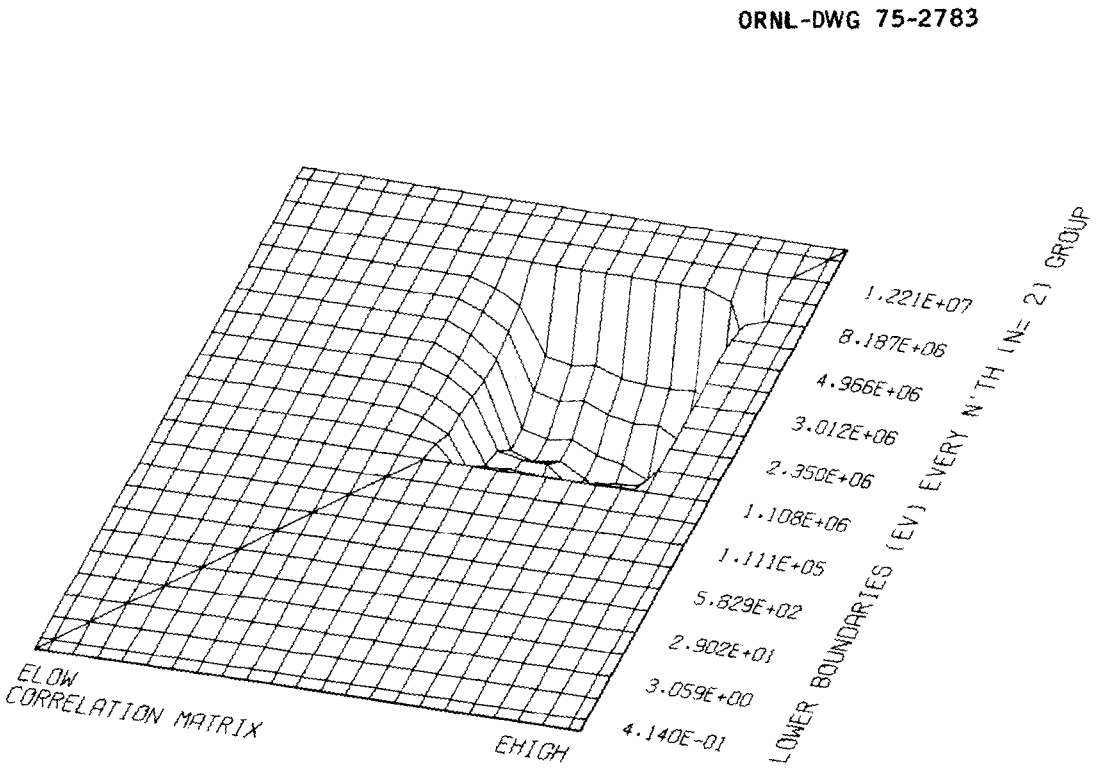

Fig. 8. Correlation Matrix as a Function of Energy Between the ^{14}N Elastic and (n,α) Cross Section.

and only slightly less so at higher energies (∿5-8%). The cross section is not fully correlated, as assumed in ref. 2 (with only the limited information available at that time) and there is some structure clearly evident. Above 1 MeV, the correlation matrix tends to become more diagonal with increasing energy; at lower energies (<600 eV) the full correlation assumption appears valid.

Figure 7 illustrates the same type of behavior exhibited in the (n,α) cross section. Where the standard deviation curve goes outside the plot frame, the uncertainty has become inordinately large. This typically is the case for a reaction near threshold. The standard deviation is of the order of (20-30%) and is not fully correlated. It is the diagonal elements that are primarily important for the description of the inelastic (reaction 4), capture (reaction 102), and (n,p) (reaction 103) cross sections above 600 eV. Below this energy, both capture and (n,p) are fully correlated functions of energy. Figure 8 illustrates the correlation matrix as a function of energy for cross-section covariance. The "deep" hole indicates the anti-correlation between elastic and (n,α) below 10 MeV [to preserve the total cross section, if the elastic cross section increases, the (n,α) would decrease etc.]. The "grand canyon" has significant structure and is not uniformly -1 across the entire energy range as assumed in ref. 2.

The process of folding these covariance matrices with sensitivity profiles is described in Section VI.

V. UNCERTAINTIES INTRODUCED IN THE AVERAGING OF MULTIGROUP CROSS SECTIONS

The neutron multigroup cross sections used in the energy grid selection phase of the study were processed using the XLACS module of the AMPX system[16] while those used in the final analysis of the 266-group benchmark were obtained with the MINX[14] code. Both programs are available at ORNL and the choice was made primarily for expediency. However this, and more fundamental interest, does raise the question of consistency

and validity of different multigroup processing techniques. Significant differences due to a wide variety of distinct physical approximations in flux modeling and methods of numerically group averaging have already been reported for fast reactor situations.[7]

To investigate the potential impact of cross-section processing methods uncertainties, the benchmark was repeated using MINX (M) multigroup data, XLACS (X) multigroup data, and pointwise cross sections used in conjunction with the point-ANISN (PA) technique.[4] The integrated boundary fluxes obtained were 0.925 (PA), 0.835 (M), and 0.784 (X) neut/sec. The volume of the detector zone is that corresponding to the last of the 201 spatial intervals. The point-ANISN results are expected to be on the high side because the points on the chosen grid emphasize minima in the total cross section and do not use averages of σ_T. This approach tends to increase the response for deep penetration problems compared with that obtained using multigroup methods. Approximately six percent differences in the integrated boundary flux are presently attributed exclusively to differences in multigroup processing techniques. Using a linear perturbation theory estimate, $\Delta R/R$ is estimated by:

$$(\Delta R/R)_X = \sum_G P_{X,G}(\Delta\sigma/\sigma)_{X,G} \tag{18}$$

$$(\Delta R/R) = \sum_X (\Delta R/R)_X \tag{19}$$

where

$P_{X,G}$ = relative sensitivity coefficient, reaction X group G,

$(\Delta\sigma/\sigma)_{X,G}$ = relative difference in multigroup cross sections for reaction X, group G,

$(\Delta R/R)_X$ = projected change in response due to a change in multigroup cross-section type X.

We find that essentially all the 6% difference comes in the processing of multigroup transfer matrices. Differences arising from processing integrated cross section (e.g., σ_{el}, σ_{in}) lead to changes in response

which are less than .2% most of this coming from the linearization approximation in MINX.

VI. FOLDING NUCLEAR DATA COVARIANCE MATRICES WITH SENSITIVITY PROFILES

The 266-group forward and adjoint fluxes computed in Section III have been combined to generate sensitivity profiles[2] for all important reaction cross sections in air. As an example, Fig. 9 illustrates the profile for the (n,α) cross section for ^{14}N. The complete set of profiles were then folded with the relative covariance matrices generated in Section IV according to the following equation:

$$\left(\frac{\Delta R}{R}\right)^2 = \sum_{X,Y,G,H} P_{X,G} \text{ Rel. Cov. } (X_G, Y_H) \; P_{Y,H} \tag{20}$$

with the following definitions

$P_{X,G}$ = relative sensitivity profile for reaction X, group G,

$\left(\frac{\Delta R}{R}\right)^2$ = relative variance due to nuclear data uncertainties in integrated reaction cross sections.

Tables V and VI present the results of this folding process. The summation has been partitioned in thirds to distinguish the contribution from a given reaction Z, how it correlates with all other reactions, and the contributions from all terms not involving reactions Z. The individual reactions are enumerated below:

Reaction Number	Reaction Type
2	σ_{el}
4	σ_{in}
102	$\sigma_{n,\gamma}$
103	$\sigma_{n,p}$
107	$\sigma_{n,\alpha}$

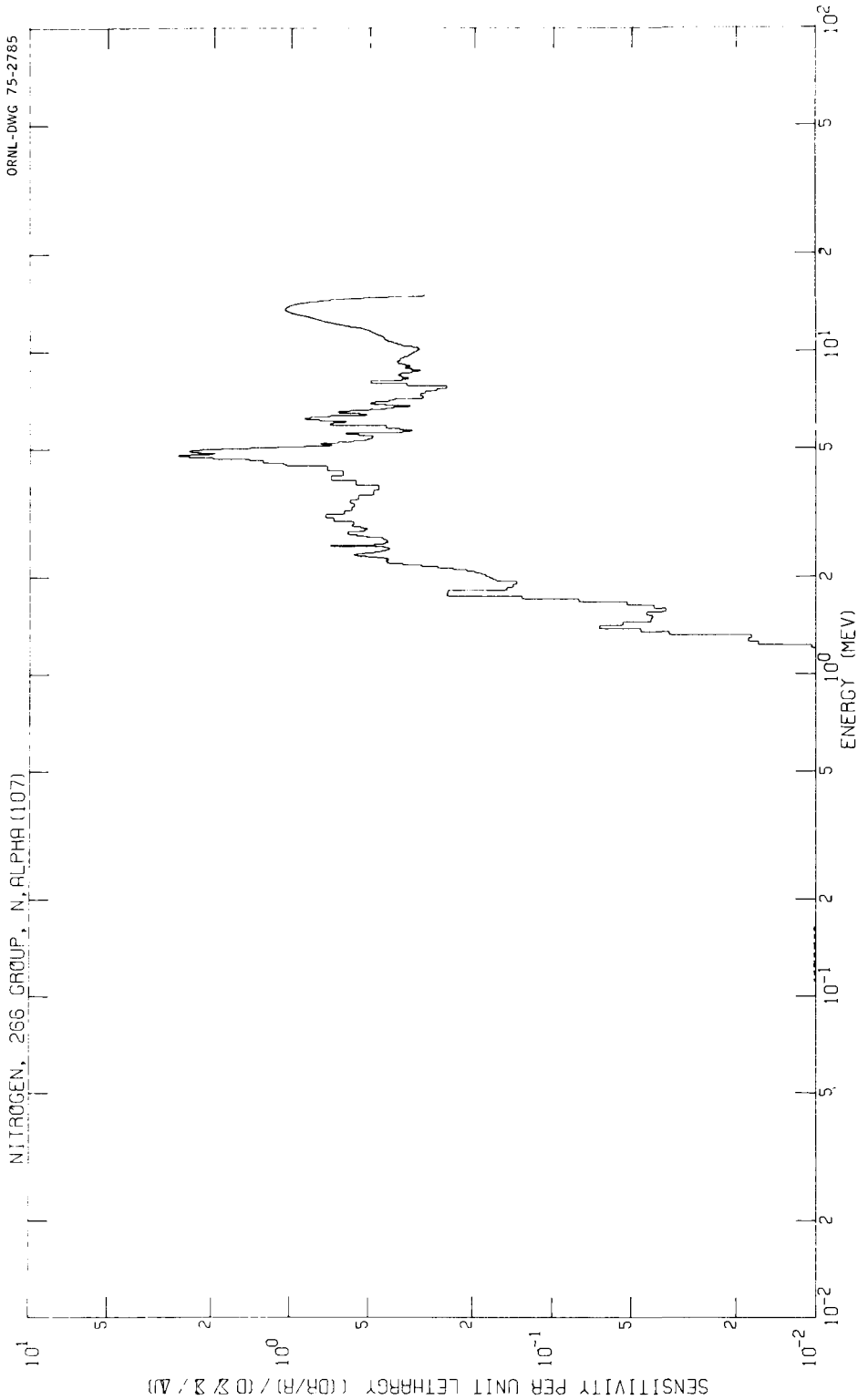

Fig. 9. Sensitivity Profile for the $^{14}N(n,\alpha)$ Cross Section.

Table V. Components to the Variance of the Integrated Boundary Fluence due to Nuclear Data Uncertainties in ^{14}N (MAT 1275)

Variance Component	ENDF/B IV	Uncorrelated	Fully Correlated
React 2 → 2	4.518+1	1.038+0	2.182+2
React 2 → others	-2.147+2	-5.506+0	2.168+3
All react 2	-1.696+2	-4.468+0	2.386+3
Not react 2	4.532+2	1.326+1	5.387+3
React 4 → 4	7.805+1	4.835+0	5.211+2
React 4 → others	-5.294+1	-3.807+0	2.983+3
All react 4	2.512+1	1.028+0	3.504+3
Not react 4	2.585+2	7.761+0	4.269+3
React 102 → 102	4.675-4	2.657-5	4.664-3
React 102 → others	0	0	1.203+1
All react 102	4.675-4	2.657-5	1.204+1
Not react 102	2.836+2	8.789+0	7.761+3
React 103 → 103	1.916+1	9.377-1	1.578+2
React 103 → others	-1.368+1	-6.514-1	1.899+3
All react 103	5.486+0	2.863-1	2.057+3
Not react 103	2.781+2	8.502+0	5.716+3
React 107 → 107	3.812+2	9.379+0	1.439+3
React 107 → others	-1.985+2	-4.838+0	3.811+3
All react 107	1.826+2	4.541+0	5.250+3
Not react 107	1.010+2	4.247+0	2.523+3
Relative standard deviation ^{14}N cross section uncertainties (%)	1.684+1	2.964+0	8.816+1

Table VI. Components to the Variance of the Integrated Boundary Fluence due to Nuclear Data Uncertainties in ^{16}O (MAT 1276)

Variance Component	ENDF/B IV	Uncorrelated	Fully Correlated
React 2 → 2	1.723+0	7.356-2	1.365+1
React 2 → others	-2.473+0	-2.080-1	7.410+1
All react 2	-7.502-1	-1.344-1	8.775+1
Not react 2	5.385+0	4.319-1	1.006+2
React 4 → 4	3.490+0	3.435-1	3.224+1
React 4 → others	-2.275+0	-2.119-1	9.136+1
All react 4	1.215+0	1.317-1	1.236+2
Not react 4	3.420+0	1.858-1	6.471+1
React 103 → 103	4.179-2	5.016-3	2.438-1
React 103 → others	-4.248-2	-3.833-3	1.306+1
All react 103	-6.889-4	1.184-3	1.331+1
Not react 103	4.635+0	2.963-1	1.750+2
React 107 → 107	2.427+0	1.222-1	1.487+1
React 107 → others	-1.304+0	-6.997-2	7.609+1
All react 107	1.123+0	5.223-2	9.097+1
Not react 107	3.512+0	2.453-1	9.734+1
Relative standard deviation from ^{16}O cross section uncertainties (%)	2.152+0	5.455-1	1.372+1

Since covariance matrices for all the integrated reaction cross sections (including those quantities derived) were explicitly given in the ENDF/B-IV file, we have chosen to consider each of the partials as the independent reaction cross section; thus, the total cross section appears only implicitly in Tables V and VI.

Assuming no correlation between the N and O uncertainty files, the relative standard deviation due to all integrated reaction cross-section uncertainties is 17.0%. The importance of the ^{14}N (n,α) cross section is clearly evident, as it was in earlier studies. Just as clear is the relative unimportance of ^{16}O cross sections. The ^{14}N elastic cross section is anti-correlated with other reactions diminishing the contribution to the variance from the uncertainties in the elastic scattering cross section considered by itself. As a function of energy, the "Uncorrelated" case corresponds to no correlation between cross sections in different energy groups; correlation between reactions for a given energy group is still included. "Fully Correlated" corresponds to the case of unity everywhere in the correlation matrix. These latter two cases are included simply to give the reader a feeling for the sensitivity of the estimated overall uncertainty due to two extreme kinds of correlation evaluation.

VII. COMPARISON OF TRANSPORT METHODS

The point and multigroup discrete ordinates results obtained above have been compared to fluxes calculated using the moments method technique. This latter procedure was one of the earliest methods applied to deep penetration radiation transport problems in simplified geometry of uniform composition. Modern moments method[17] and flux reconstruction[18] programs are very fast (the 267 energy point air problem, including cross-section preparation, runs in less than three minutes in the ORNL 360/91) and compute the infinite medium spectrum, the age, higher moments (up to 20.0), and the flux of all spatial and energy points in the system including all cross-section detail.

We have found that the total integrated fluxes agrees to within 1% at all space points out to 1000 meters. At 1500 meters, differences of the order of 7% are observed. The fluxes right at the boundary cannot be easily compared since the moments technique applies only to infinite media. However, for higher energy groups (e.g., 12.2-14.9 MeV), where the angular flux is primarily outward directed, the two techniques give fluxes at 2000 meters which agree to within 7%. Finally, detailed comparisons of flux spectra at individual space points were unconclusive due to non-physical structure in the moments method fluxes at specific energy points due primarily to failure of a particular reconstruction scheme. In general, however, the moments method spectra agree well with the benchmark results. The agreement in spatial behavior with the flux averaged over broad energy bins is also good.

VIII. CONCLUSIONS

Sensitivity analysis is applied to the study of an air transport benchmark calculation to quantify and distinguish between cross section and method uncertainties. The boundary detector response was converged with respect to spatial and angular mesh size, P_ℓ expansion of the scattering kernel, and the number and location of energy grid boundaries. The uncertainty in the detector response due to uncertainties in nuclear data is 17.0% (one standard deviation, not including uncertainties in energy and angular distribution) based upon the ENDF/B-IV "error files." Differences of approximately 6% can be attributed exclusively to differences in processing multigroup transfer matrices. The formal documentation of the PUFF computer program for the generation of multigroup covariance matrices is presented.

REFERENCES

1. E. G. Silver, E. M. Oblow, J. M. Kallfelz, C. R. Weisbin, D. E. Bartine, G. F. Flanagan, and F. R. Mynatt, "Generalized Reactor Sensitivity Program at ORNL," Trans. Am. Nucl. Soc. 18, 341 (June 1974).

2. D. E. Bartine, E. M. Oblow, and F. R. Mynatt, "Radiation Transport Cross-Section Sensitivity Analysis - A General Approach Illustrated for a Thermonuclear Source in Air," Nucl. Sci. Eng., 55, 147-167 (1974).

3. E. M. Oblow, D. E. Bartine, and F. R. Mynatt, "General Sensitivity Theory for Radiation Transport," ORNL-TM-4110 (March 1973).

4. J. Ching, H. Goldstein, and E. M. Oblow, "Application of a Discrete-Energy Discrete-Ordinates Technique to the Study of Neutron Transport in Iron," ORNL-TM-4235 (December 1974).

5. E. Oblow, J. Ching, and J. Drischler, "Selection of Group Energy Boundaries Using Sensitivity Theory," Trans. Am. Nucl. Soc. 17. 547 (1973).

6. F. G. Perey, G. deSaussure, and R. B. Perez, "Estimated Data Covariance Files for Evaluated Cross Sections - Examples for ^{235}U and ^{238}U," Proceedings of ANS Topical - Advanced Reactors: Physics, Design, and Economics, September, 1974, to be published.

7. C. R. Weisbin, N. M. Greene, H. Henryson, II, R. J. LaBauve, C. Durston, D. E. Cullen, and R. B. Kidman, "Fast Reactor Cross-Section Processing Codes - Is There a Dollars Worth of Difference Between Them?" Proceedings of ANS Topical - Advanced Reactors: Physics, Design, and Economics, September, 1974, to be published.

8. D. E. Bartine, F. R. Mynatt, and E. M. Oblow, "SWANLAKE, A Computer Code Utilizing ANISN Radiation Transport Calculations for Cross-Section Sensitivity Analysis," ORNL-TM-3809 (May 1973).

9. W. W. Engle, Jr., "A User's Manual for ANISN, A One-Dimensional Discrete Ordinates Transport Code with Anisotropic Scattering," K-1693, Computing Technology Center, Oak Ridge Gaseous Diffusion Plant (1967).

10. F. Perey, Format Modifications 73-7, minutes of the CSEWG meeting, December 1973 (enclosures 6 and 12).

11. F. G. Perey, "The Estimated Data Covariance Files of ENDF/B - Their Uses," minutes of the CSEWG meeting, June 17-19, 1974 (enclosure 10).

12. H. Henryson, II et al., "Variational Sensitivity Analysis - Theory and Application," Proceedings of ANS Topical - Advanced Reactors: Physics, Design, and Economics, September, 1974, to be published.

13. C. R. Weisbin, "PUFF, An ENDF/B-IV Error File Processing Code," ORNL Quarterly Report to the Defense Nuclear Agency (April 1974).

14. C. R. Weisbin, P. D. Soran, R. E. MacFarlane, D. R. Harris, R. J. LaBauve, J. S. Hendricks, and J. E. White, "MINX, A Multigroup Interpretation of Nuclear Cross Sections from ENDF/B," Los Alamos Scientific Laboratory (to be published); see also, Trans. Am. Nucl. Soc., 16, 127 (1973).

15. F. G. Perey, "Tedium Isotopes for MF=33," correspondence to the Error Quantity Subcommittee of the CSEWG (May 29, 1974).

16. N. M. Greene and F. R. Mynatt, "The AMPX Modular Code System for Generating Coupled Neutron-Gamma Multigroup Cross-Section Sets," Trans. Am. Nucl. Soc., 15, 568 (1972); see also, N. M. Greene et al., "AMPX: A Modular Code System for Generating Coupled Multigroup Neutron-Gamma Libraries from ENDF/B," ORNL-TM-3706 (to be published).

17. C. R. Weisbin, H. Goldstein, and L. J. Lidofsky, Trans. Am. Nucl. Soc., 12, 402 (1969); see also, "A New Moments Solution to the Neutron Transport Equation," NYO-268, Pegram Nuclear Physics Lab (1969).

18. P. D. Soran, "Reconstruction of Neutron Spatial Distribution from Spatial Moments," Columbia University Doctoral Thesis, 1971.

ACKNOWLEDGEMENTS

The authors take great pleasure in acknowledging the efforts of D. K. Trubey in making the moments method technique operational and getting appropriate solutions for this problem. F. G. Perey and P. G. Young made significant contributions in the review and application of the ENDF/B-IV error files. Virginia Glidewell deserves many thanks for preparing this manuscript in the appropriate format.

APPENDIX A

AN UPDATE OF AN EARLIER AIR TRANSPORT SENSITIVITY ANALYSIS (BASED ON REF. 2) USING ENDF/B-IV COVARIANCE FILES

The tissue dose uncertainty is presently calculated as a factor of two lower than that quoted in the Bartine, Oblow, Mynatt study [NSE 55, 157 (1974) made without the benefit of the present ENDF/B-IV detailed covariance files] using identical 101/33 coupled sensitivity coefficients. As seen in Table A.1, the (n,α) cross section still dominates (although not as much as before) but the total uncertainty is only $\sim$14.5% (1 standard deviation) based upon uncertainties in the smooth cross sections, including gamma-ray production, but ignoring uncertainties in energy and angular distributions, gamma-ray multiplicities, and gamma-ray interaction cross sections.

With a goal of calculating air transport to 25%, it is clear that an accurate remeasurement of the $N(n,\alpha)$ cross section can reduce the variance in the tissue dose well below the desired goal. However, *if* the uncertainties in the present file are reasonable estimates, and *if* the uncertainties in the spectral and angular distribution data are less important, then the required goal has very nearly been met today without further work. It would be prudent, however, to go ahead with the measurement program since the importance of the aforementioned *ifs* would then be diminished and only a single measurement is involved.

Table A.1. Uncertainty Analysis for Air Transport from Prototypic Thermonuclear Source (2000 meters)

MATERIAL 1275 ENDF/B-4 FILE Nitrogen Covariances

	ENDF/B-4	UNCORRELATED	FULLY CORRELATED
REACT 2 TO REACT 2[a]	2.83747E C1	2.43638E 00	1.32918E 02
REACT 2 TO OTHERS	-1.16247E C2	-1.04003E 01	1.13995E 03
ALL REACT 2	-8.78720E C1	-7.56387E 00	1.27287E 03
NOT REACT 2	2.96603E C2	2.73701E 01	2.44415E 03
REACT 4 TO REACT 4[b]	2.81605E C1	9.64877E 00	1.62012E 02
REACT 4 TO OTHERS	-1.69327E C1	-6.97806E 00	1.22801E 03
ALL REACT 4	9.22784E CC	2.67071E 00	1.39002E 03
NOT REACT 4	1.99503E C2	1.67355E 01	2.32699E 03
REACT 102 TO REACT 102	1.85318E CC	5.25540E-01	1.76663E 00
REACT 102 TO OTHERS	0.0	0.0	-1.65603E 02
ALL REACT 102	1.85318E CC	5.25540E-01	-1.63836E 02
NOT REACT 102	2.06877E C2	1.88807E 01	3.88085E 03
REACT 103 TO REACT 103	1.69513E C1	3.79795E 00	1.18033E 02
REACT 103 TO OTHERS	-7.75758E C0	-1.36236E 00	1.08867E 03
ALL REACT 103	9.19370E C0	2.43559E 00	1.20670E 03
NOT REACT 103	1.99537E C2	1.69706E 01	2.51031E 03
REACT 107 TO REACT 107	2.58984E C2	1.67773E 01	7.38464E 02
REACT 107 TO OTHERS	-1.06249E C2	-8.81880E 00	1.83662E 03
ALL REACT 107	1.52735E C2	7.95852E 00	2.57508E 03
NOT REACT 107	5.59953E C1	1.14477E 01	1.14194E 03
TOTAL %	1.44475E C1	4.40525E 00	6.09673E 01

(14.45% uncertainty [1σ] due to nitrogen cross sections)

Total uncertainty obtained by taking the square root of the sum of ALL REACT X and NOT REACT X for any X (X = 2, 4,...., etc.) presented above.

Table A.1 (Cont'd.)

MATERIAL 1276 ENDF/B-4 FILE Oxygen Covariances

	ENDF/B-4	UNCORRELATED	FULLY CORRELATED
REACT 2 TO REACT 2	1.28215E CC	1.49503E-01	7.01423E 00
REACT 2 TO OTHERS	-1.54582E CC	-4.54213E-01	3.54233E 01
ALL REACT 2	-2.63625E-C1	-3.44710E-01	4.24375E 01
NOT REACT 2	3.23EC4E CC	1.C6588E 00	4.47235E 01
REACT 4 TO REACT 4	1.52242E CC	8.16111E-01	1.50538E 01
REACT 4 TO OTHERS	-1.1C782E CC	-4.52543E-01	4.23384E 01
ALL REACT 4	6.146C6E-C1	3.63567E-01	5.73921E 01
NOT REACT 4	2.15581E CC	3.57599E-01	2.57689E 01
REACT 103 TO REACT 103	1.447C0E-C2	8.38052E-03	4.82013E-02
REACT 103 TO OTHERS	-9.47E63E-C3	-6.14304E-03	4.C0300E 00
ALL REACT 103	4.5513EE-C3	2.23748E-03	4.05120E 00
NOT REACT 103	2.56542E CC	7.18929E-01	8.31098E 01
REACT 107 TO REACT 107	1.40E74E C0	3.C0150E-01	6.69827E 00
REACT 107 TO OTHERS	-6.39714E-C1	-1.53057E-01	3.49285E 01
ALL REACT 107	7.67C32E-C1	1.47C94E-01	4.16268E 01
NOT REACT 107	2.2C73EE CC	5.74072E-01	4.55343E 01
TOTAL %	1.72465E CC	6.49215E-01	9.33600E 00

(1.72% uncertainty [1σ] due to oxygen cross sections)

[a]Reaction types: 2 - elastic
4 - inelastic
102 - capture
103 - (n,p)
107 - (n,α)

[b]Uncertainty in the inelastic cross section assumed uniformly distributed between levels.

APPENDIX B

A PROGRAMMER'S GUIDE FOR THE PUFF UNCERTAINTY FILE PROCESSING CODE

The PUFF processor was written to extend the capabilities of the MINX multigroup processing code to include the ENDF/B-IV uncertainty files. Multigroup covariance matrices are constructed according to Eqs. (8-11).

According to ENDF/B-IV formats, error file information is located at the end (file 33) of the description for a given material. However, in order to implement Eqs. (8-11), the energy "edges" used in File 33 must be available early in the calculation to compute the required multigroup cross sections on the unionized grid (between the user group structure and the energy grid used in the error file description). It was therefore decided to retrieve and store the error file information in a pre-processing stage; for MINX this naturally corresponds to the reconstruction of point-wise cross sections from resonance parameters. If processing begins from a PENDF tape, error file BCD data is then read separately from the original ENDF/B tape (unit 20). Table B-1 lists the format in which error file data is presently stored. Such information is then retrieved when the multigroup structure is established. Once the super grid is formulated, multigroup processing proceeds in the usual fashion with the energy grid, group fluxes, and cross sections appropriately stored for the actual error processing at a later stage. Table B-2 lists the format in which the user energy grid, fluxes, and cross sections are presently stored. Since the supergroup structure is composed of the union between the user group structure and all energies used in the error file description, the number of groups can obviously get very large quite rapidly as the size of the problem considered and the level of detail available in the files expand. The large number of fluxes and cross sections required have been appropriately labelled (see Table B-2 - Format for Energy Grid, Group Flux, and Cross Section Scratch Disk Storage) for subsequent automated retrieval. Note that most processing codes normally do not preserve group flux values. The need for allowing dimensions to easily expand at a later date clearly required the programming to be within a variable dimensioning formalism.

With the error file data, fluxes, and cross sections appropriately stored and labelled, the computation of the covariance matrix is reduced to a direct collapsing procedure with weights determined directly from the error files. The only real problem is to keep track of energy indices; there is a user energy grid, a supergrid including the union of the user grid with boundaries contained in all error subsections, and finally N grids representing the union of the user grid and the energy bounds in the m^{th} error subsection of the p^{th} reaction (N = pm).

This calculation has been successfully implemented for each of the four covariance representations conceived (e.g., fully correlated with energy-dependent magnitude). The programming philosophy was to make this new coding transparent to the MINX non-error file user, i.e., new programming did not impose any additional significant restraint (e.g., storage) on the main MINX processing function.

Block flow diagrams and flow diagrams by subroutine are presented in Figs. B-1 and B-2, respectively; the latter being primarily those MINX subroutines required for the error processing functions. The covariance matrix for each reaction of a given material is generated as a function of energy, one reaction at a time. Additional capability implemented in PUFF was the ability to process only selected reactions corresponding to those for which covariance files have been constructed (i.e., NOREAC option). After all reactions have been processed, the covariance matrices between reactions for a given material are generated. Lastly, covariance between materials is considered. Table B-3 lists the major change to the MINX subroutines. Particular variable definitions are presented in Table B-4. The program input is listed in Table B-5; the output of the code is described in Table B-6. Table B-7 lists the present error processing code limitations.

The program has been verified by successful processing of the ERRIUM isotopes,[17] hand calculations, and comparisons with results from an independent program.[6]

Table B-1. Format for Error Files, Scratch Disk Storage

Quantity	Routine	Unit	Mode	Format
Error File Data	DELTA	33	Binary	(MAT1,MT1,NC,NI,MATH,MFH,MTH) (LT,LB,NP2,NP) (CWERR(J),J=1,NP2) — Repeat NI+NC times Repeat for all sections in a given MTH, including cross MT Repeat for all MTH MZERO,MZERO,MZERO,MZERO,MZERO,MZERO,MZERO MATEND,MZERO,MZERO,MZERO,MZERO,MZERO,MZERO

Note: MZERO = 1000
MATEND = 10000

Table B-2. Format for User Energy Grid, Group Flux, and Cross Section Scratch Disk Storage

Quantity	Routine	Unit	Mode	Format
User Energy Grid	RUSEG	NSCRR (22)	Binary	WRITE(NSCRR),NEN,(ESXSE(J),J=1,NEN)
Fluxes	INTXS	NSCRR (22)	Binary	WRITE(NSCRR)(CENOM(JCW),JCW=1,NGPS)
Cross Sections	GRUPXS	NSCRR (22)	Binary	WRITE(NSCRR),MATNOW,MT, TMPNOW,SIG,NGPS(X(J),J=1,NGPS)

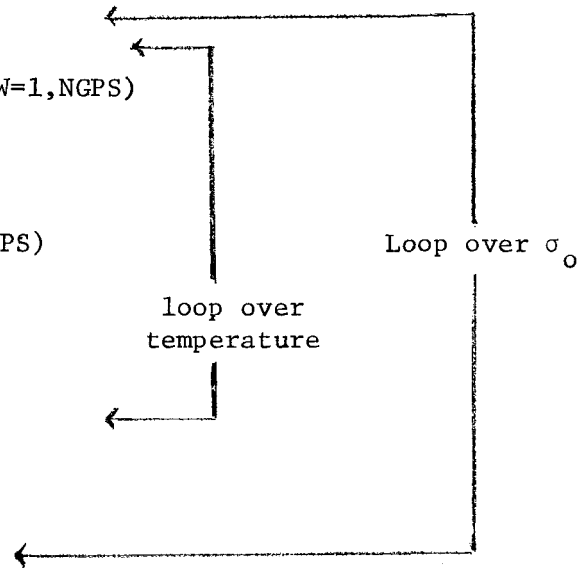

[a]Read in DANNY.

[b]When processing covariance for same reaction, go sequentially through cross sections on disk file; for cross reaction covariance, go sequentially through reactions on error data file.

Table B-3. Major Changes to the MINX Subroutines to Include Error Processing

1. Labelled commons - MTNAME and DIANNE moved to (4,0) from (4,2).
2. MAIN - Comment version number, date, and limitations.
3. Odelli
   a) coding to read and print error flag
   b) introduction of commons /CONTR/ and /LERROR/
4. XSGEN
   a) bring a common /LERROR/
   b) specify the length of blank common
5. CFEND
   a) introduction of common /LERROR/
   b) test to see if you need to CALL DELTA to read the error information while copying to the end of the tape
   c) if error data is read, turn off flag MMERR so no attempt is made to read it again when CFEND is called from other routines (e.g., SIGMA1)
   d) terminate read on end of material
6. DELTA - completely new routine
   a) if error flag is on, read uncertainty data and store on unit 33
   b) present coding limits input error files to BCD
   c) avoid unnecessary copy if in tape restart mode
7. COPYCW - completely new routine
   a) copy the error file data to unit 12 along with the rest of the cross-section information in BCD format
8. TERROR
   a) adjusted to call DANNY if error flag is on
   b) allow restart from a pointwise tape

Table B-3 (Cont'd.)

9. RUIN

   a) call RUSEG with storage available for x and y to accommodate super-group structure
   b) minor change in call statement to RUSEG

10. RUSEG

   a) If error flag is on, write the user group structure onto NSCRR; defines NSCRR-22 and rewinds
   b) form the unionized grid reading error data from unit 33 and print
   c) subroutine statement arguments modified
   d) commons /LERROR/ and /UNITS/ added

11. GRUPXS

   a) write multigroup cross sections in unionized structure onto NSCRR
   b) use MAT=10000 for indication of end of tape file
   c) add commons /LERROR/ and /CONTR/
   d) turn on group cross-section printer conditionally with error flag MERR; otherwise print later after collapse
   e) implement options to process only selected reactions (i.e., NOREAC option)

12. INTXS

   a) write the integrated group fluxes in super-group structure onto NSCRR
   b) add common /CONTR/

13. DANNY - completely new routine

   a) reads scratch file for user group structure
   b) loops on T and σ_o; retrieves fluxes and cross sections and prints collapsed results
   c) terminates on MATNOW=10000
   d) calls SUMMF to do the collapsing to user group structure
   e) allocates pointers for dimensions and storage allocation
   f) calls PUFF for the actual covariance matrix calculation
   g) calls INVT to invert matrices and invoke symmetry

Table B-3 (Cont'd.)

h) calls WOT for print of results - covariance matrices, correlation matrices and relative quantities

i) indicate successful termination of processing

j) output in BCD on unit 7

14. WOT

a) print routine which is different from the WOT used in regular MINX

15. INVT - completely new routine

a) inverts matrices by group (high energy becomes group 1)

b) invokes symmetry where applicable

16. PUFF - completely new routine

a) performs the covariance matrix calculation once all input is established in DANNY

17. SUMMF - completely new routine

a) collapses fluxes and cross sections for super-group structure to user structure

Table B-4. Important Variable Definitions

1. PHIKUN(ϕ_{kun}) - Supergroup flux for a structure corresponding to the union of the user energy grid and the energy structure E_k for n^{th} subsection.
2. GMTKUN (G_{MT}^{kun}) - Multigroup cross section for reaction MT in the same structure as that described for PHIKUN (HMTKUN is the same definition for group H, reaction MT).
3. EKUN - Energy boundaries for the same structure as that described in PHIKUN.
4. ENPTS - Energy bounds for the super-group structure which contains the overlap of the user boundaries and <u>all</u> energy edges described in any subsection for any reaction of interest.
5. ESXSE - Energy boundaries of the user group structure.
6. ESXS - Multigroup cross sections in the user structure.
7. COVMT - Covariance matrix for the material-reaction pairs; it is a two-dimensional array with energy in each direction.
8. FKUN - uncertainty component data for the same energy grid as described for PHIKUN.
9. NENG - Number of groups in the user grid.
10. NGPS - Number of groups in the largest supergroup structure.
11. POINTERS

INITIAL	FINAL	VARIABLE
K1	J2	COVMT
J4	J5	Std. dev. for 1st reaction
J6	J7	Std. dev. for 2nd reaction
J8	J9	Std. dev. for 3rd reaction
J10	J11	Std. dev. for 4th reaction
J12	J13	Std. dev. for 5th reaction

Table B-4 (Cont'd.)

INITIAL	FINAL	VARIABLE
J14	J15	Std. dev. for 6th reaction
J3	K2	DAT
K3	K4	PHIKUN
K5	K6	GMTKUN
K7	K8	EKUN
K9	K10	Z
K11	K12	HMTKUN
K13	K14	Scratch space (correlation matrix, covariance matrix, relative std. dev.)
K15	K16	User x-sect. for 1st cross reaction
K17	K18	User x-sect. for 2nd cross reaction

12. MATHC, MFHC, MTHC - Material, file, and reaction of interest.

13. MMAT1, MMT1 - Material and reaction to which there is a covariance.

14. Y - Cross sections in the user group structure are stored here.

15. CENOM - Supergroup fluxes for the energy grid associated with ENPTS.

16. X - Cross sections in the super-group structure associated with EKUN.

17. NP2 - Number of entries in a given uncertainty section of ENDF/B data.

18. DAT - The actual error file data for a given section.

19. Z - Cross sections for reaction to which there is a covariance.

Table B-5. Error Processing Input Requirements

Typical PUFF Input for an ^{16}O Sample Problem

```
ERROR PROCESSING OF OXYGEN 22 GROUPS
 1275  1275     0     1      100.0       0.001       0.001       0.01
    1     1     0     1      2   23      1   1       1   5       1
    1     2     4   103   107
                                                                  1
300.0
                                                                  1
200.0
                                                                 23
 1.0      -5  4.14      -1  5.3159  -1  3.059        1.0677  +1  2.9023  +1
 1.013    +2  5.8295    +2  3.3546  +3  1.1109  +5   5.5023  +5  1.108   +6
 1.8268   +6  2.35      +6  2.466   +6  3.0119  +6   4.0657  +6  4.9659  +6
 6.36     +6  8.1873    +6  10.0    +6  12.214  +6   14.918  +6
```

Table B-6. PUFF Disk Output Description*

Quantity	Format	Description	Purpose
NENG, MATNOW, MTH,MMAT1 MMT1	WRITE(I07,26)NENG, MATNOW,MTH,MMAT1, MMT1 26 FORMAT(515)	number of user groups, material of interest, reaction of interest and material and reaction to which there is a covariance	Plot correlation matrix
ESXSE Y STDI	WRITE(I07,27)(ESXSE(I), Y(I),RSTDI,I=1,NENG) 27 FORMAT(1X,1P3E11.4)	user energy grid, group cross section, and relative standard deviation (low to high) in %	
ICW DUM	WRITE(I07,28)ICW, (DUM(II-I),I=1,NENG) 28 FORMAT(I5,12F6.2)/ (5X,12F6.2))	group number and correlation matrix	
MATNOW MTM MMAT1 MMT1	WRITE(I07,26)MATNOW, MTH,MMAT1,MMT1 26 FORMAT(515)	material and reaction of interest followed by material and reaction to which there is a covariance	
DUM	805WRITE(I07,29)(DUM(II+I), I=1,NENG) 29FORMAT(6E12.4)	relative covariance matrix	
DUM	WRITE(I07,29)(DUM(I+IK13),I=1,NENG) 29 FORMAT(6E12.4)	relative standard deviation for 1st reaction (high to low)	
DUM	WRITE(I07,29)(DUM(I+IK13),I=1,NENG)	relative standard deviation for 2nd reaction (high to low)	

*All data is written on unit I07 and written in subroutine DANNY.

Table B-7. Present PUFF Processing Limitations

1. Input required in BCD format.
2. No covariance between materials.
3. Only file 3 type information included (e.g., no provision for processing $\bar{\nu}$). The error files are numbered by adding 30 to the MF number where the quantities themselves are entered. We only process MF=33 at present.
4. No allowance for derived files.
5. Error data is assumed to span the same energy range of ENDF/B data (at least for σ_T) (10^{-5} eV to 20 MeV).
6. No provision for correlation of uncertainty in weighting spectra with uncertainty in cross section.
7. Have not formally addressed the characterization of uncertainties in the resolved and unresolved energy regions, uncertainties in angular distributions or energy distribution.

PUFF Error Processing Segment of MINX

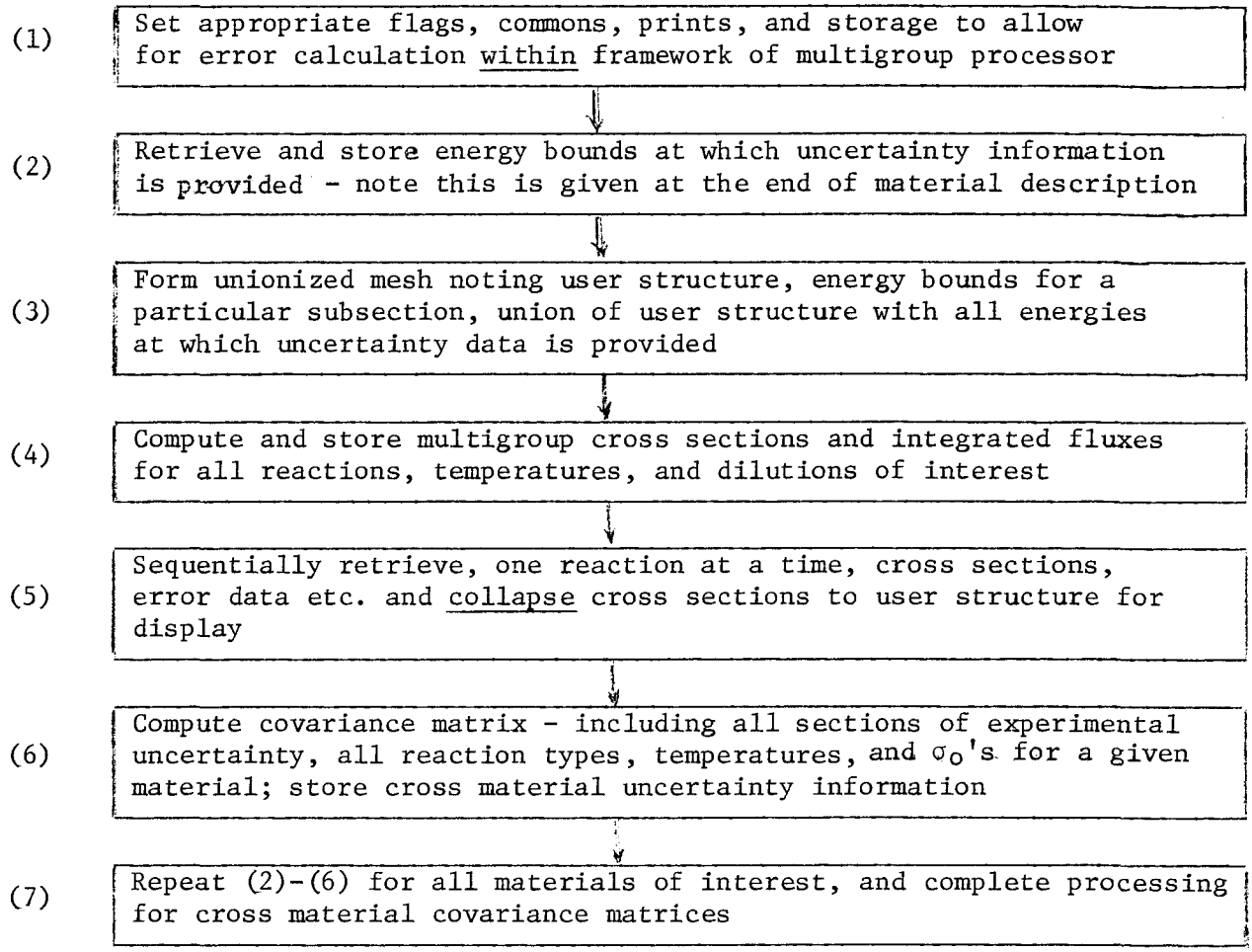

Fig. B-1. Block Flow Diagram

PUFF Error Processing Segment of MINX

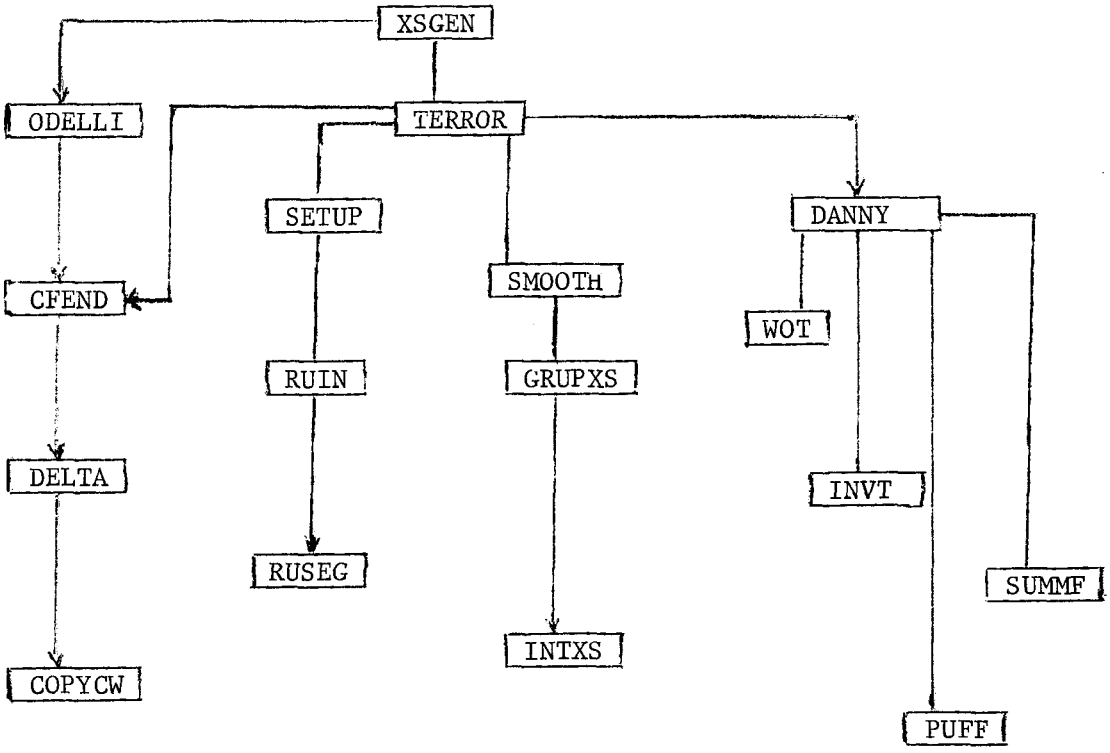

Fig. B-2. Flow Diagram by Subroutine

APPENDIX C

CORRELATION MATRICES FOR ^{14}N (MAT 1275) AND ^{16}O (MAT 1276)

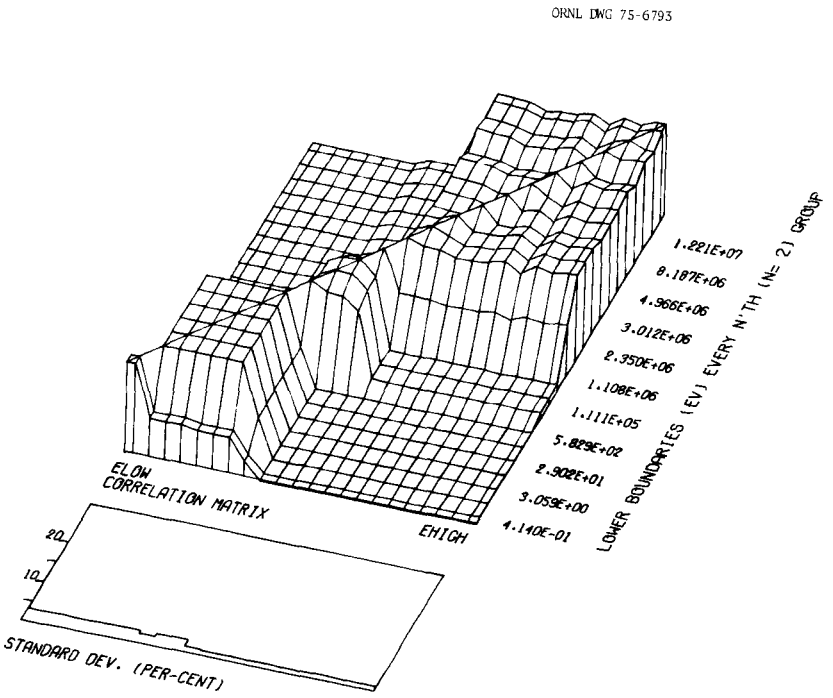

Fig. C-1. Correlation Matrix and Standard Deviation for Nitrogen Total Cross Section as a Function of Energy.

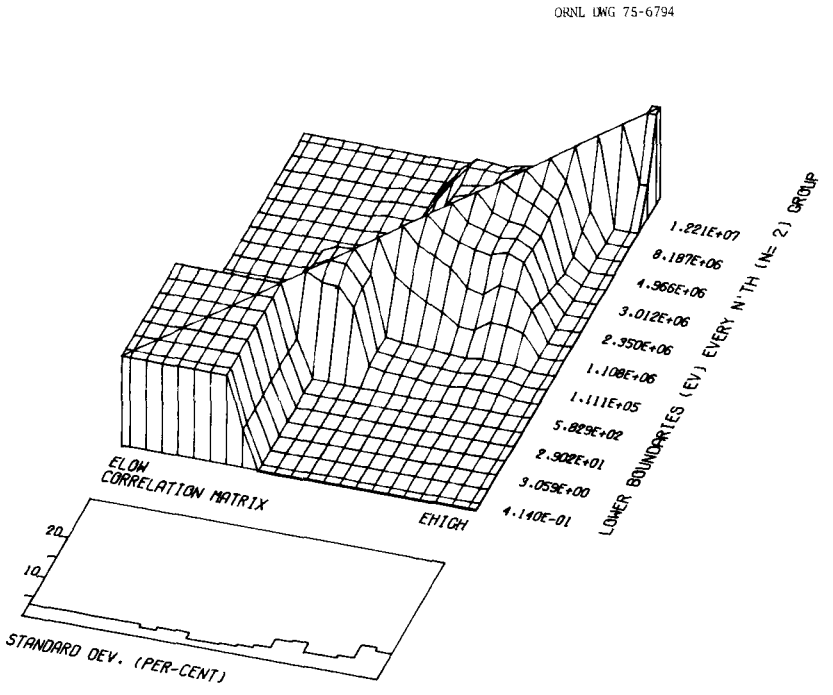

Fig. C-2. Correlation Matrix and Standard Deviation for Nitrogen Elastic Cross Section as a Function of Energy.

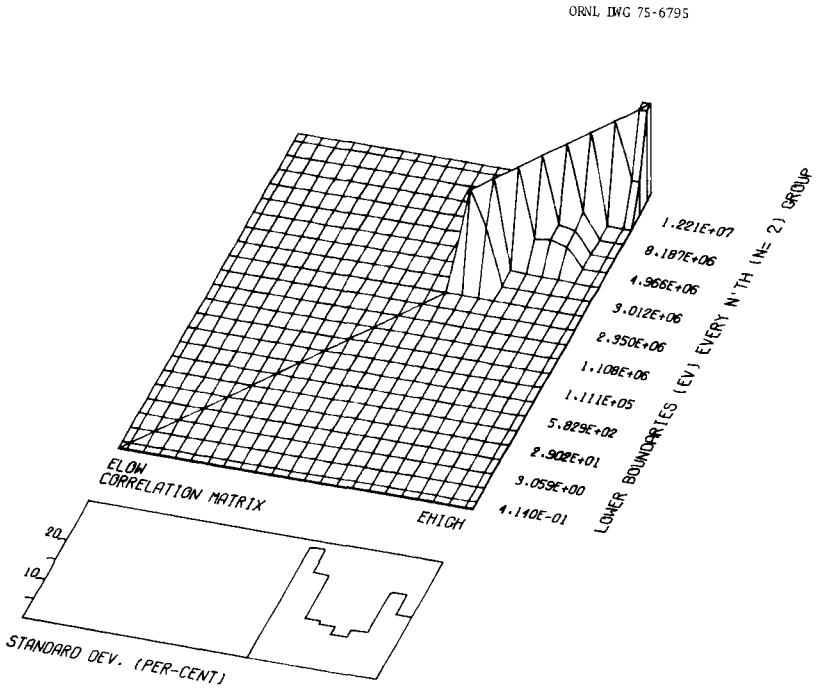

Fig. C-3. Correlation Matrix and Standard Deviation for Nitrogen Inelastic Cross Section as a Function of Energy.

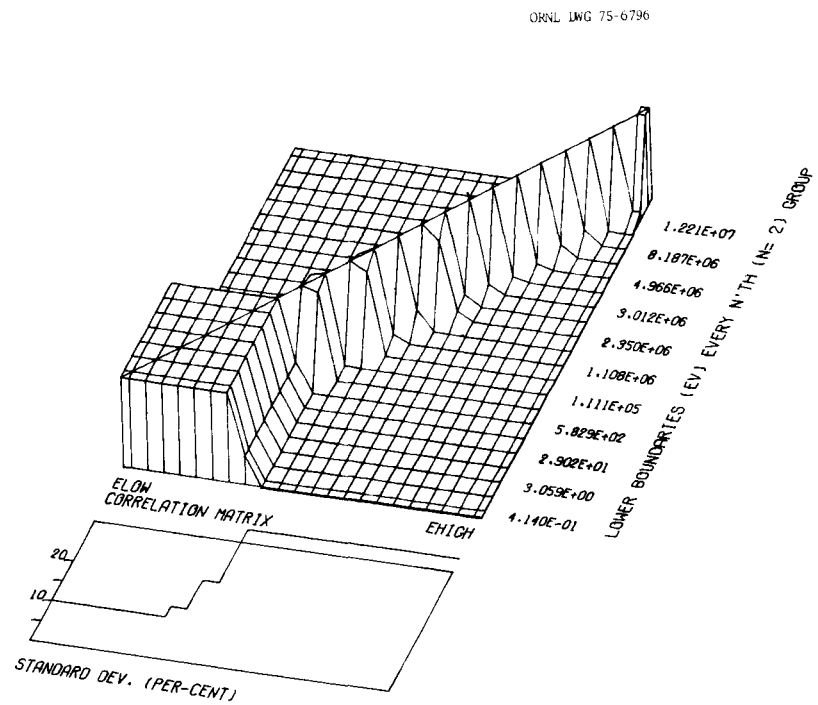

Fig. C-4. Correlation Matrix and Standard Deviation for Nitrogen Capture Cross Section as a Function of Energy.

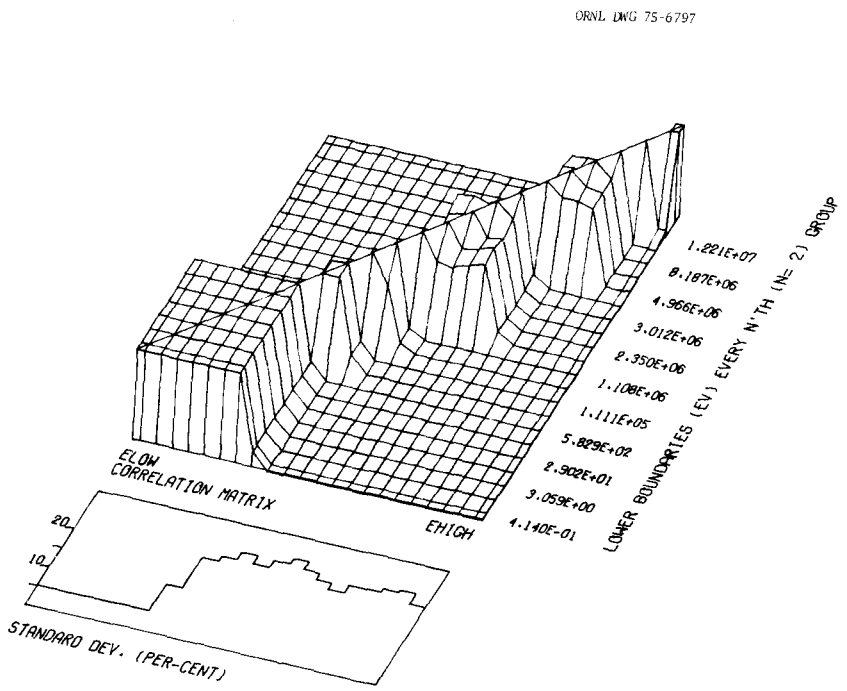

Fig. C-5. Correlation Matrix and Standard Deviation for N(n,p) Cross Section as a Function of Energy.

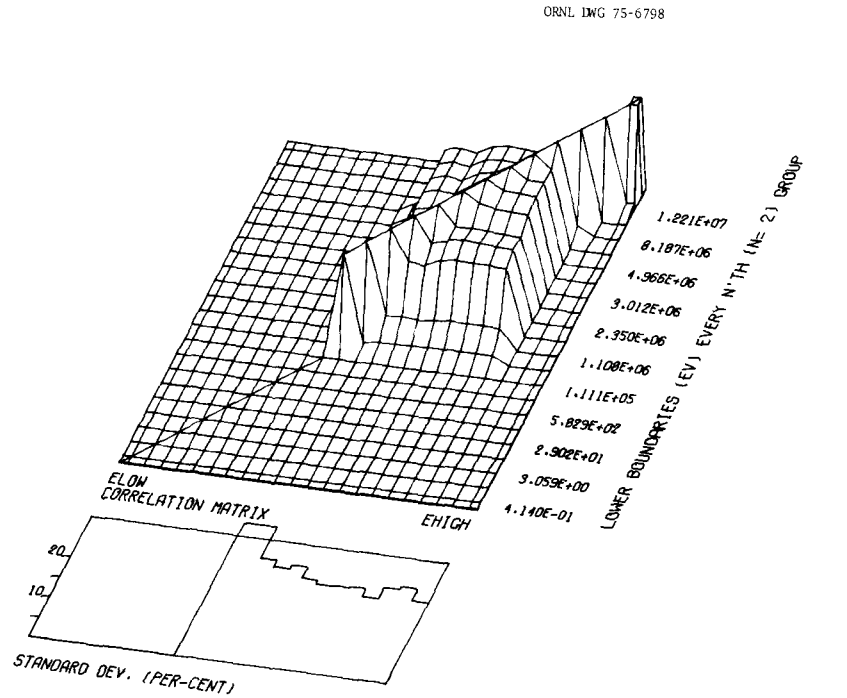

Fig. C-6. Correlation Matrix and Standard Deviation for N(n,α) Cross Section as a Function of Energy.

ORNL DWG 75-6799

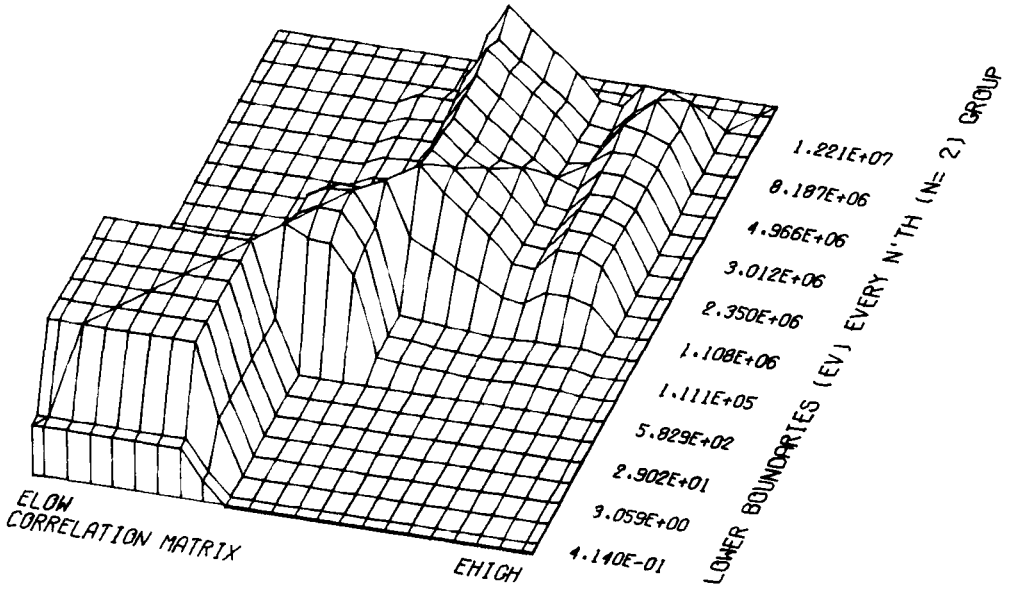

Fig. C-7. Correlation Matrix for Nitrogen Total Cross Section as It Relates to Elastic Cross Section.

ORNL DWG 75-6800

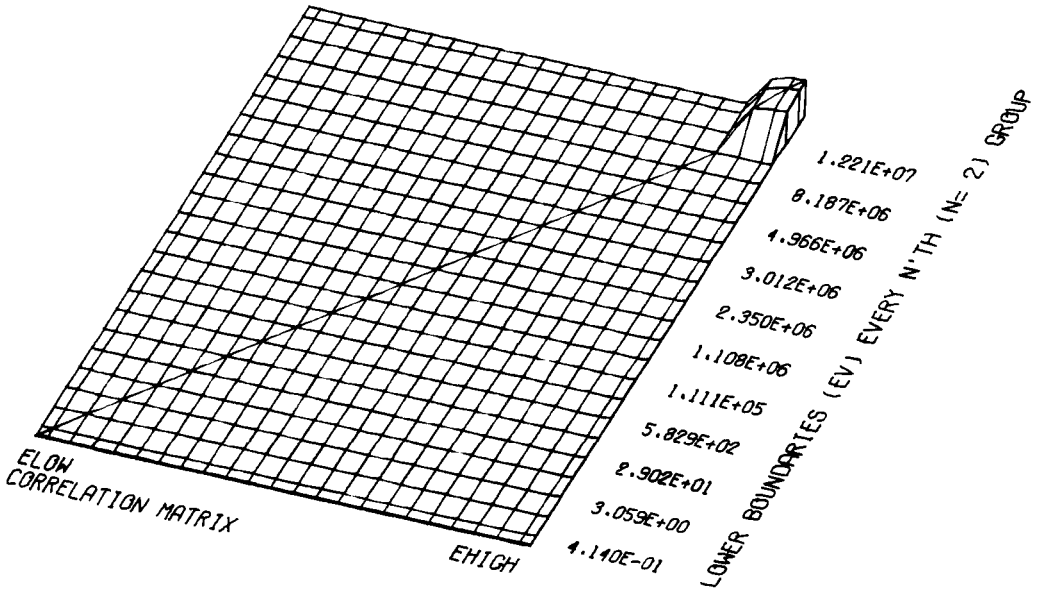

Fig. C-8. Correlation Matrix for Nitrogen Total Cross Section as It Relates to Inelastic Cross Section.

ORNL DWG 75-6801

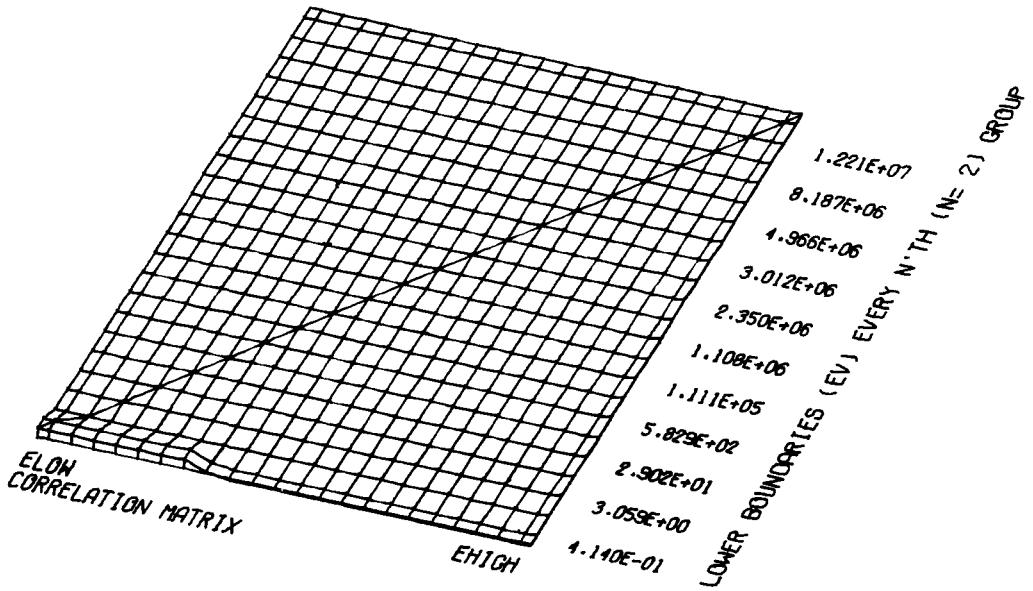

Fig. C-9. Correlation Matrix for Nitrogen Total Cross Section as It Relates to Capture Cross Section.

ORNL DWG 75-6802

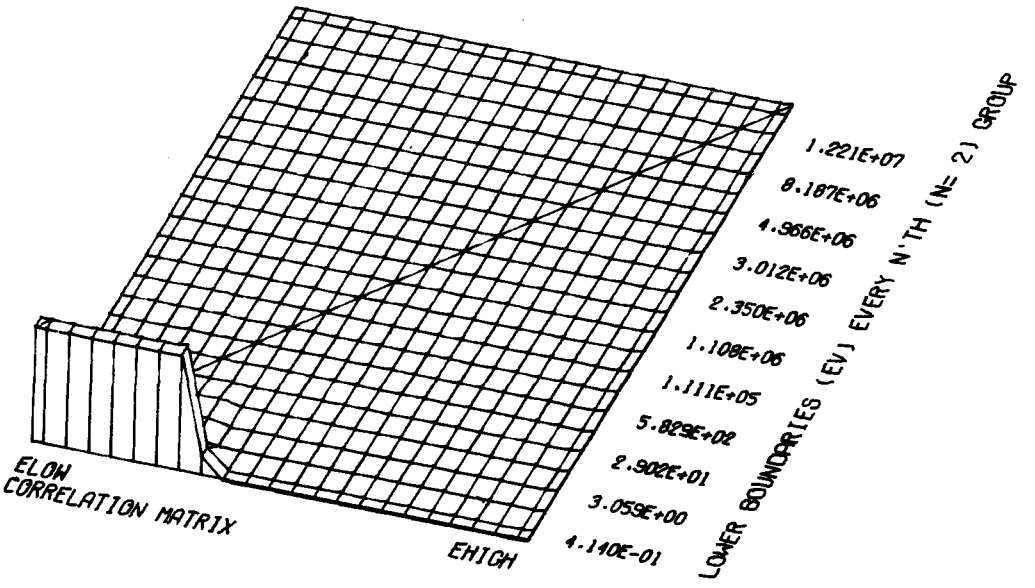

Fig. C-10. Correlation Matrix for Nitrogen Total Cross Section as It Relates to the N(n,p) Cross Section.

ORNL DWG 75-6803

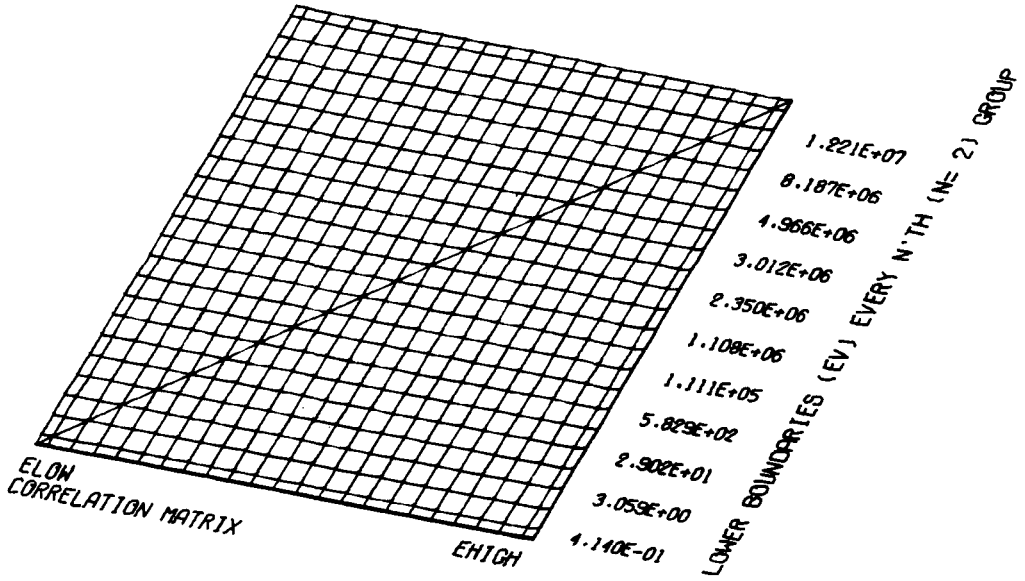

Fig. C-11. Correlation Matrix for Nitrogen Total Cross Section as It Relates to the N(n,α) Cross Section.

ORNL DWG 75-6804

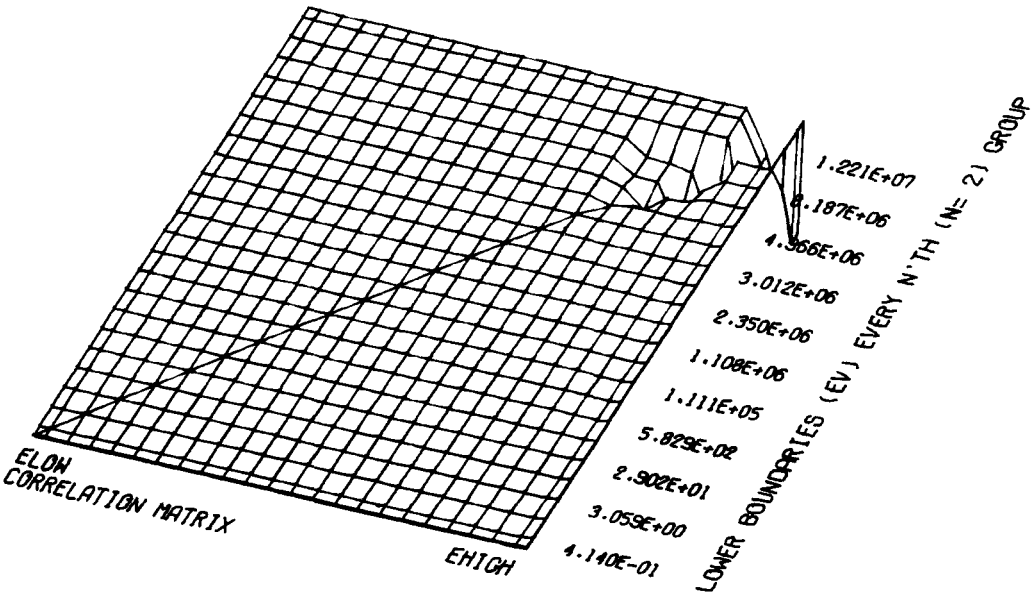

Fig. C-12. Correlation Matrix for Nitrogen Elastic Cross Section as It Relates to Inelastic Cross Section.

ORNL DWG 75-6805

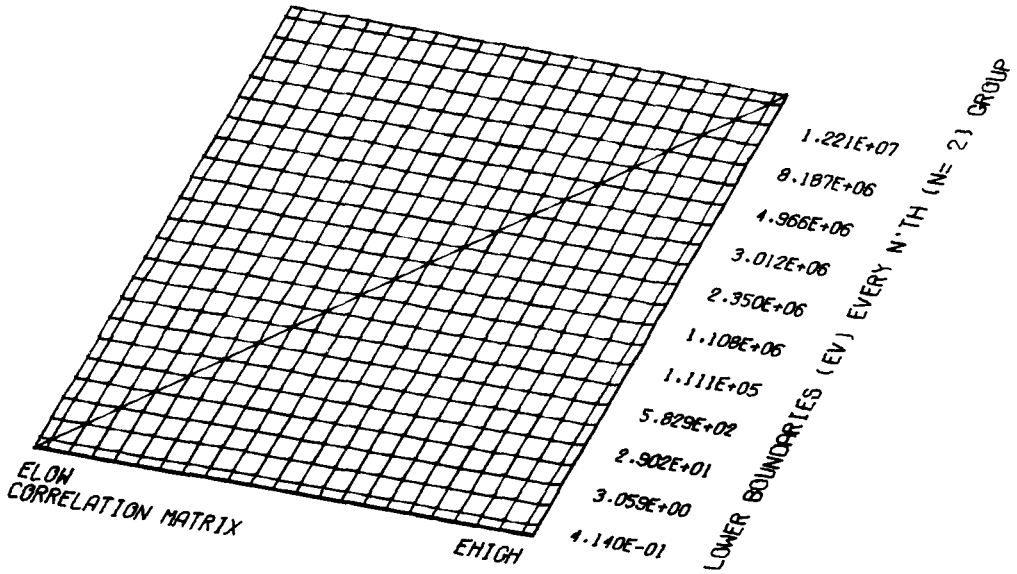

Fig. C-13. Correlation Matrix for Nitrogen Elastic Cross Section as It Relates to Capture Cross Section.

ORNL DWG 75-6806

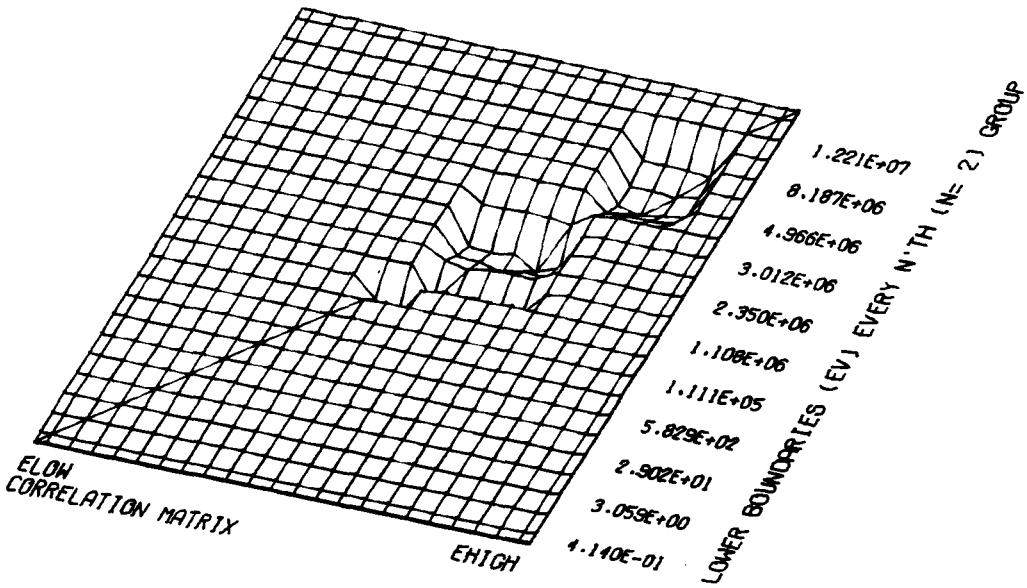

Fig. C-14. Correlation Matrix for Nitrogen Elastic Cross Section as It Relates to the N(n,p) Cross Section.

ORNL DWG 75-6807

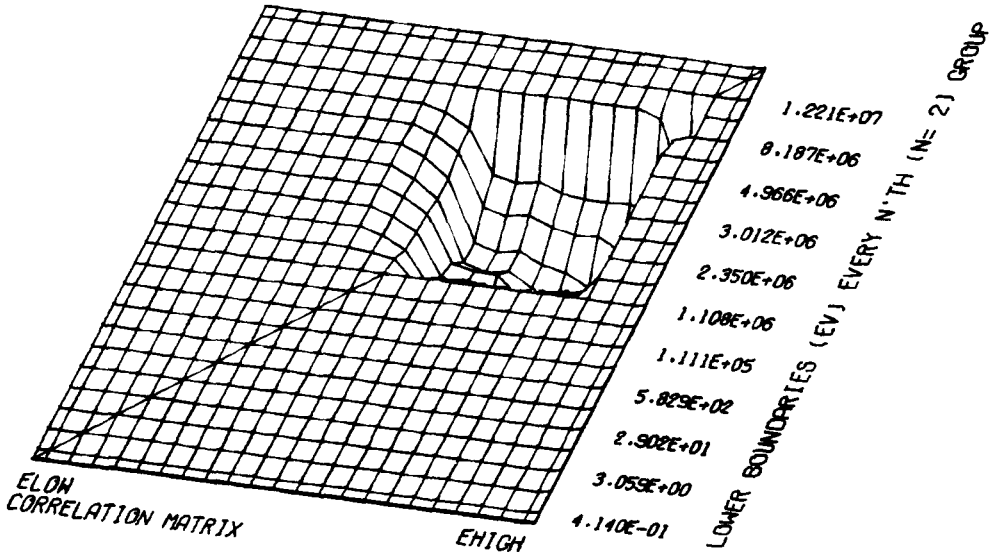

Fig. C-15. Correlation Matrix for Nitrogen Elastic Cross Section as It Relates to the N(n,α) Cross Section.

ORNL DWG 75-6808

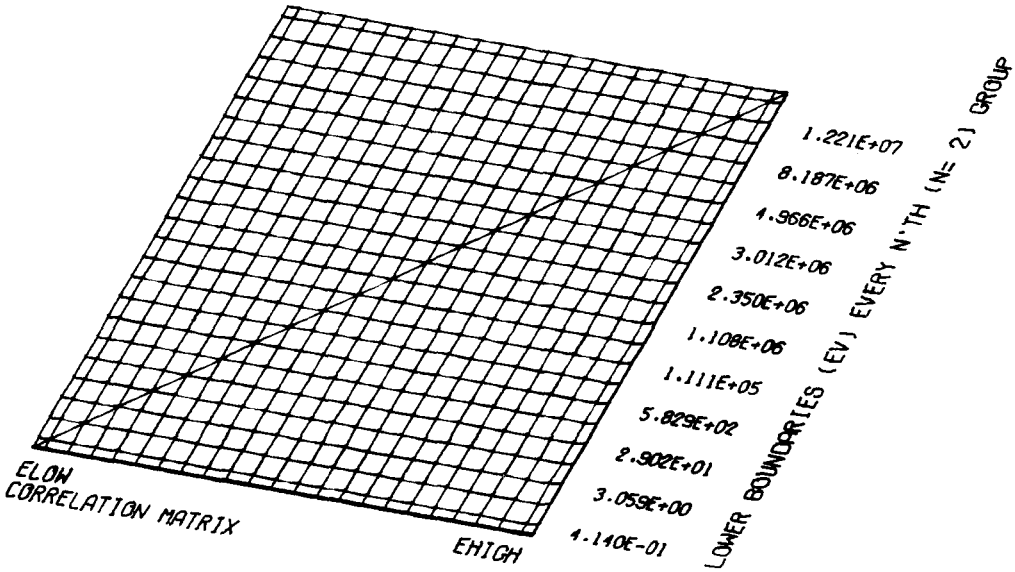

Fig. C-16. Correlation Matrix for Nitrogen Inelastic Cross Section as It Relates to Capture Cross Section.

ORNL DWG 75-6809

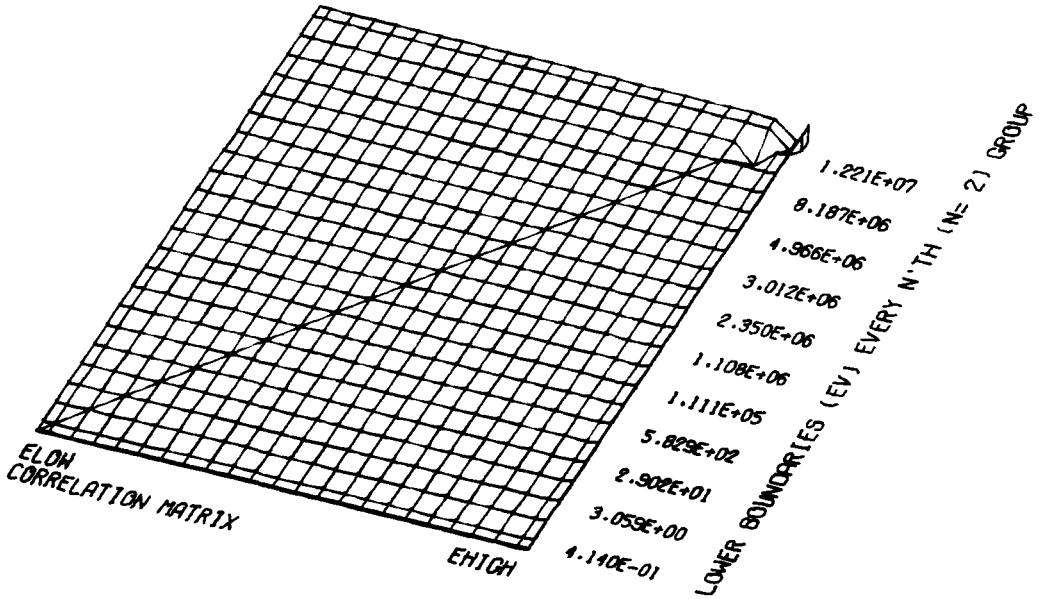

Fig. C-17. Correlation Matrix for Nitrogen Inelastic Cross Section as It Relates to the N(n,p) Cross Section.

ORNL DWG 75-6810

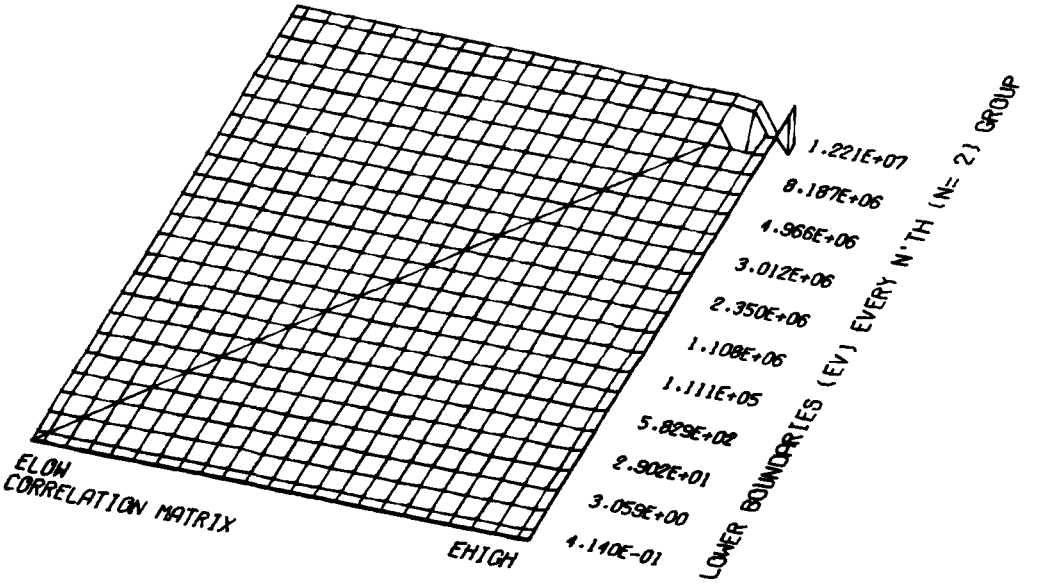

Fig. C-18. Correlation Matrix for Nitrogen Inelastic Cross Section as It Relates to the N(n,α) Cross Section.

ORNL DWG 75-6811

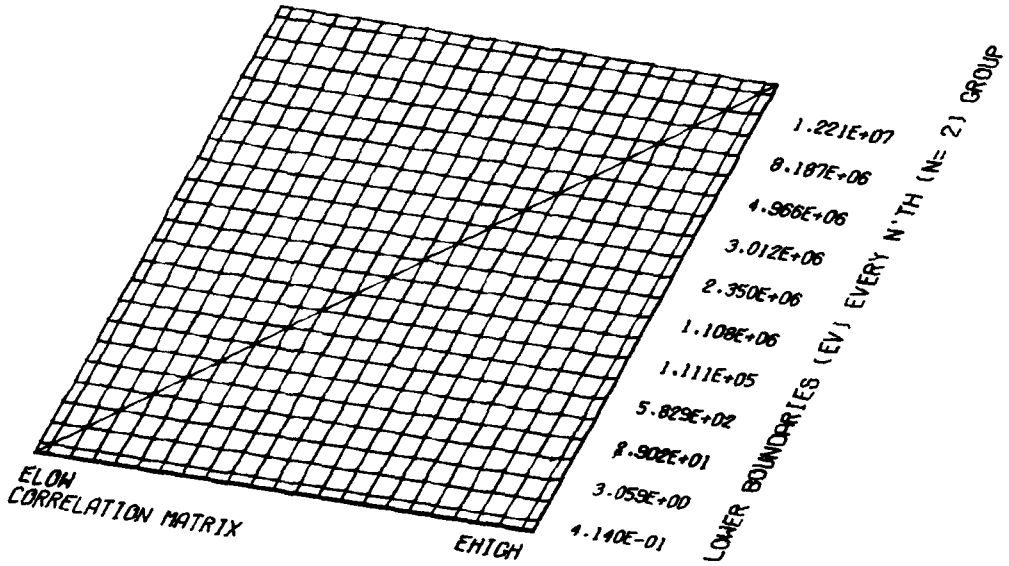

Fig. C-19. Correlation Matrix for Nitrogen Capture Cross Section as It Relates to the N(n,p) Cross Section.

ORNL DWG 75-6812

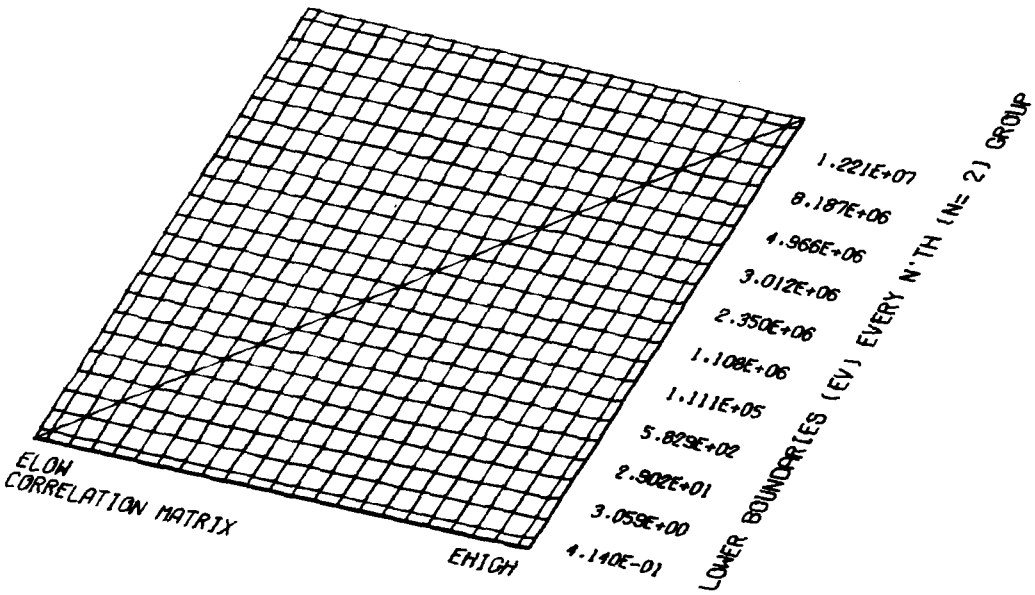

Fig. C-20. Correlation Matrix for Nitrogen Capture Cross Section as It Relates to the N(n,α) Cross Section.

ORNL DWG 75-6813

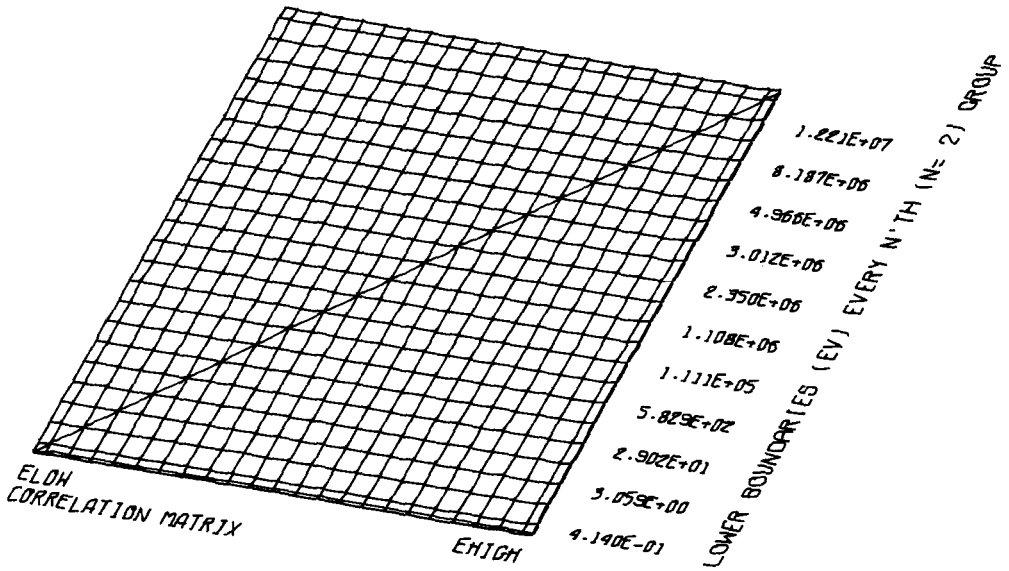

Fig. C-21. Correlation Matrix for N(n,p) Cross Section as It Relates to the N(n,α) Cross Section.

ORNL DWG 75-6814

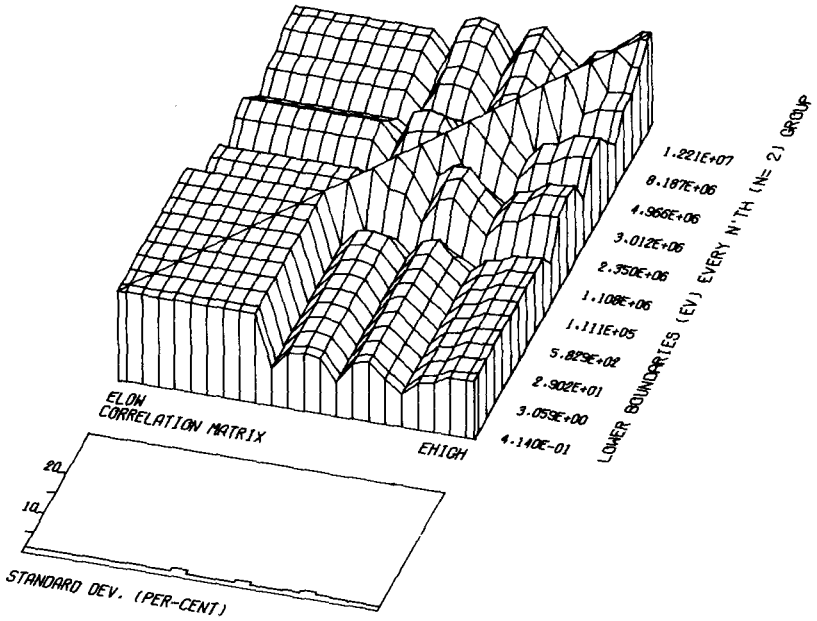

Fig. C-22. Correlation Matrix and Standard Deviation for Oxygen Total Cross Section as a Function of Energy.

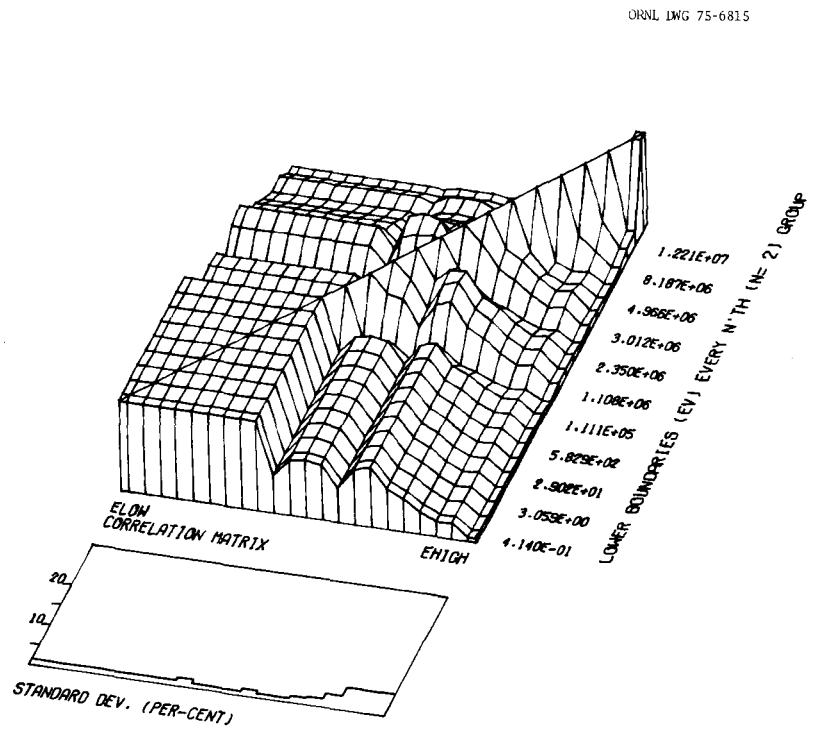

Fig. C-23. Correlation Matrix and Standard Deviation for Oxygen Elastic Cross Section as a Function of Energy.

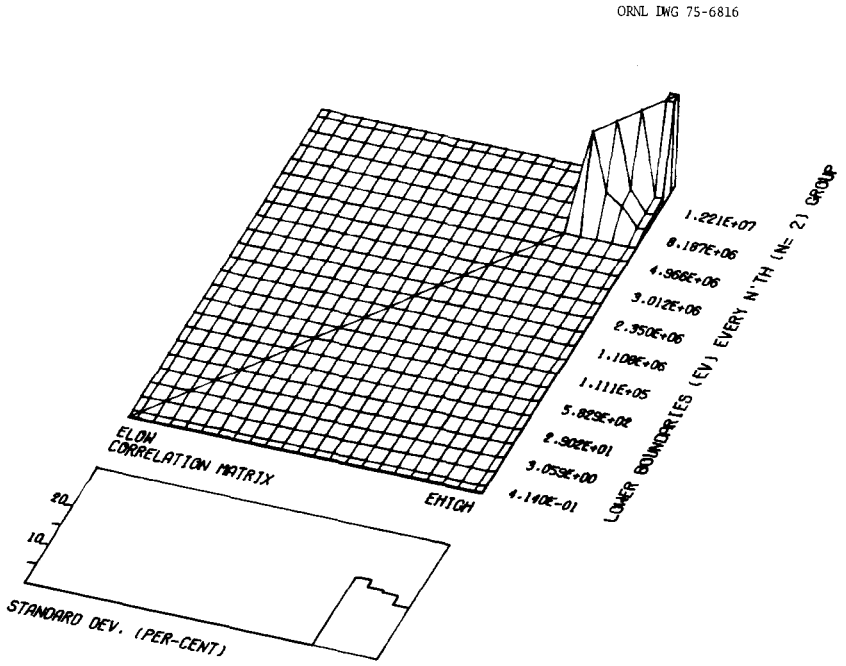

Fig. C-24. Correlation Matrix and Standard Deviation for Oxygen Inelastic Cross Section as a Function of Energy.

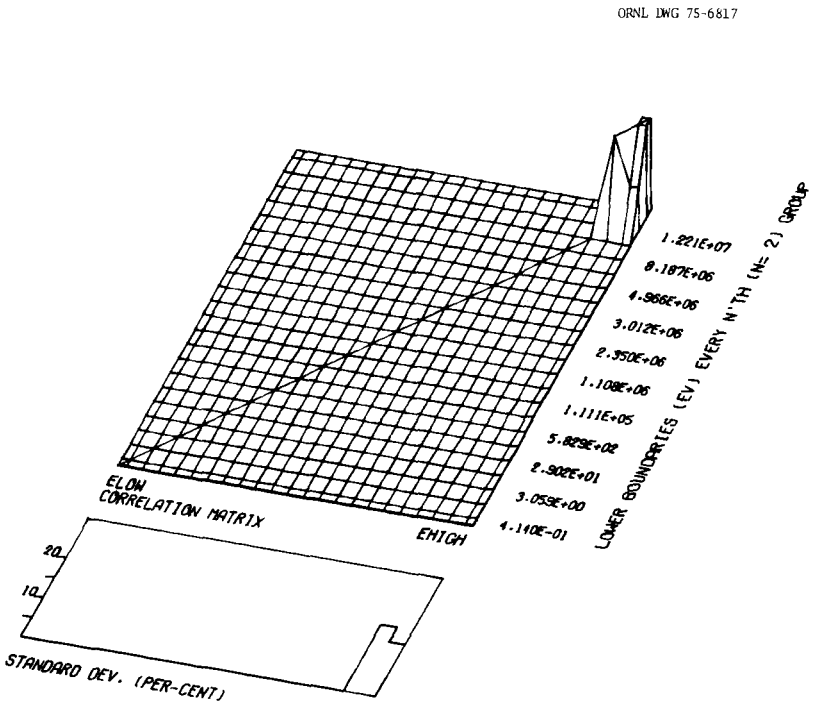

Fig. C-25. Correlation Matrix and Standard Deviation for O(n,p) Cross Section as a Function of Energy.

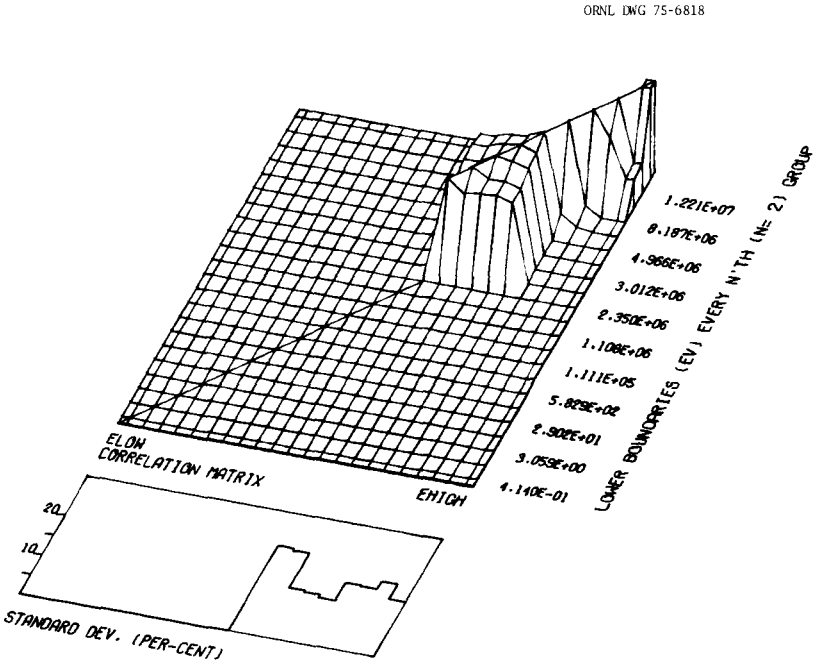

Fig. C-26. Correlation Matrix and Standard Deviation for O(n,α) Cross Section as a Function of Energy.

ORNL DWG 75-6819

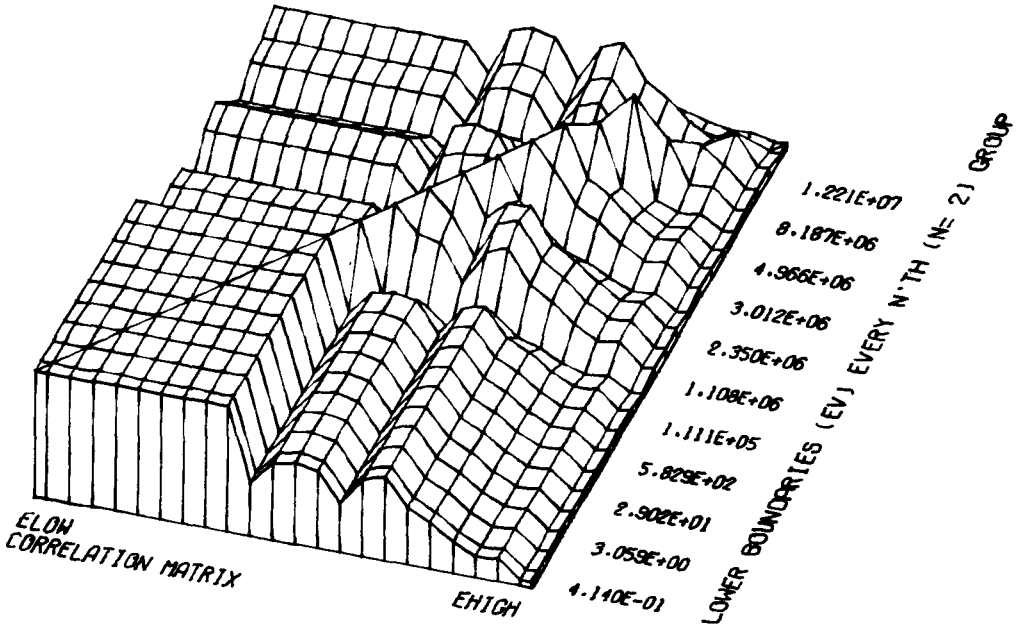

Fig. C-27. Correlation Matrix for Oxygen Total Cross Section as It Relates to Elastic Cross Section.

ORNL DWG 75-6821

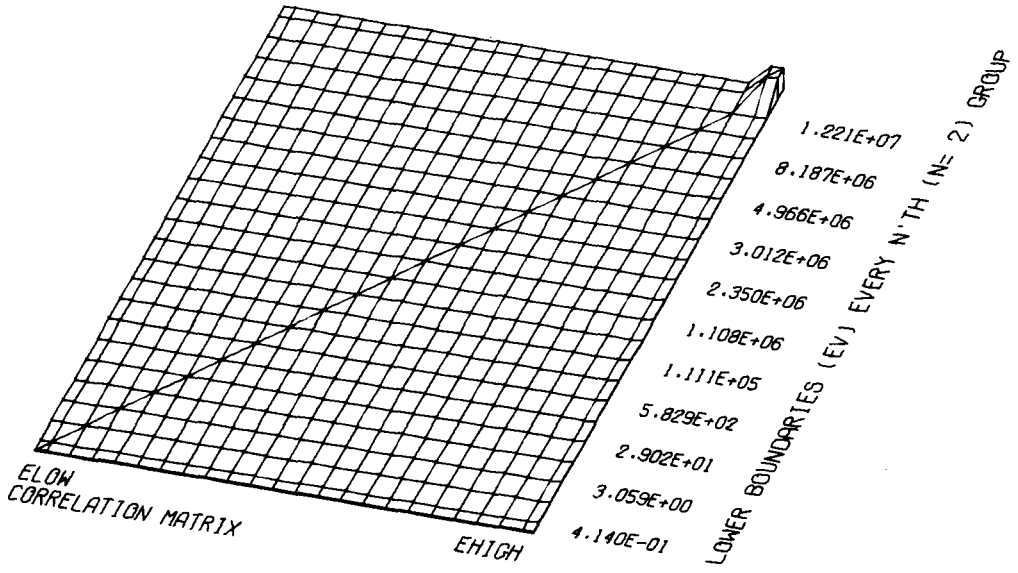

Fig. C-28. Correlation Matrix for Oxygen Total Cross Section as It Relates to Inelastic Cross Section.

ORNL DWG 75-6820

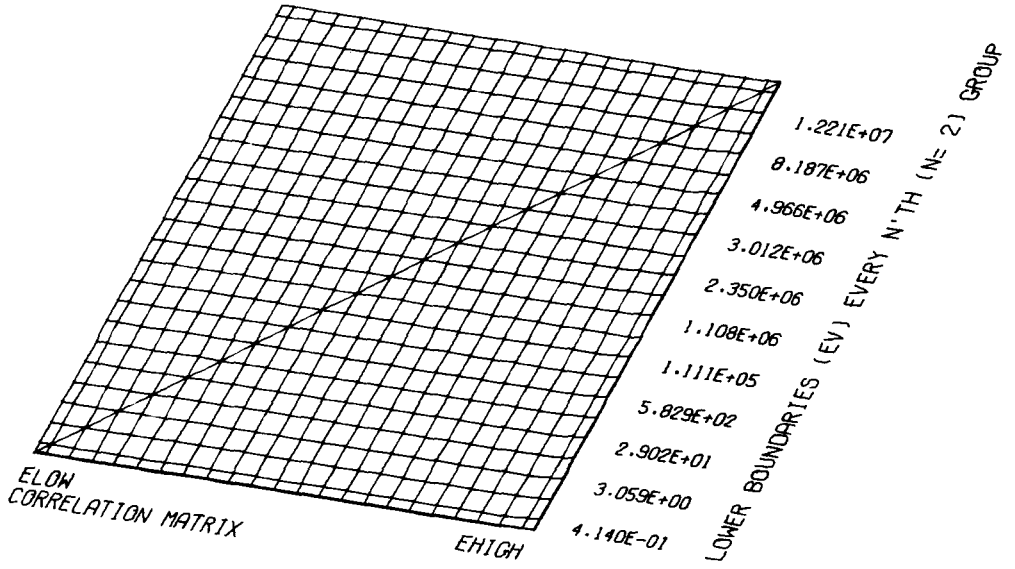

Fig. C-29. Correlation Matrix for Oxygen Total Cross Section as It Relates to the O(n,p) Cross Section.

ORNL DWG 75-6822

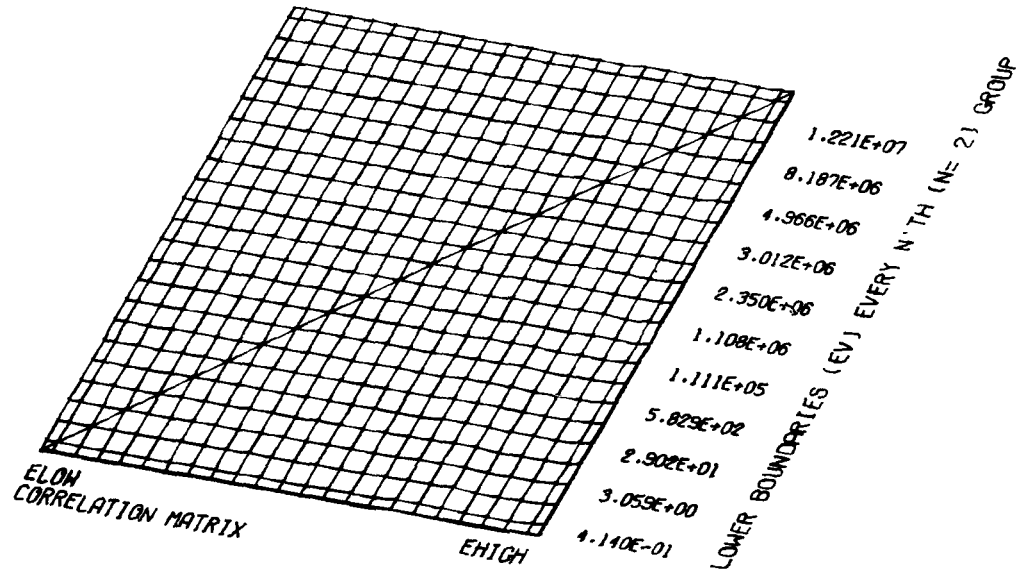

Fig. C-30. Correlation Matrix for Oxygen Total Cross Section as It Relates to the O(n,α) Cross Section.

ORNL DWG 75-6823

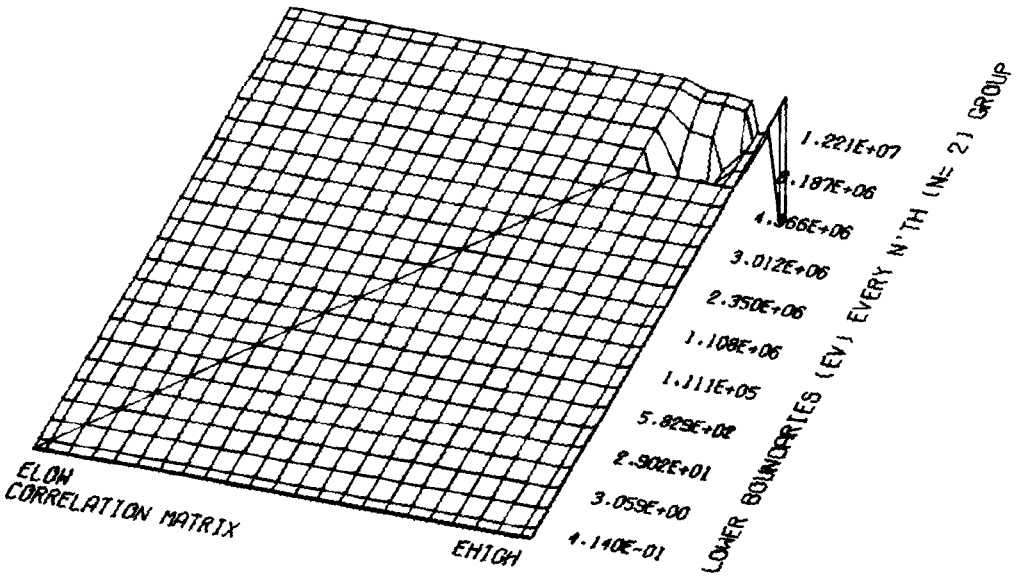

Fig. C-31. Correlation Matrix for Oxygen Elastic Cross Section as It Relates to Inelastic Cross Section.

ORNL DWG 75-6824

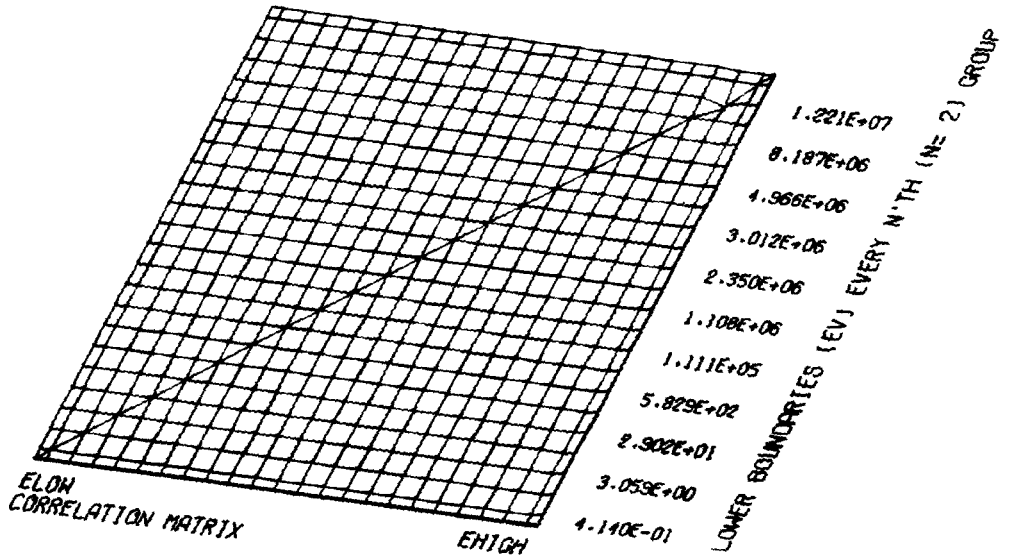

Fig. C-32. Correlation Matrix for Oxygen Elastic Cross Section as It Relates to the O(n,p) Cross Section.

ORNL DWG 75-6825

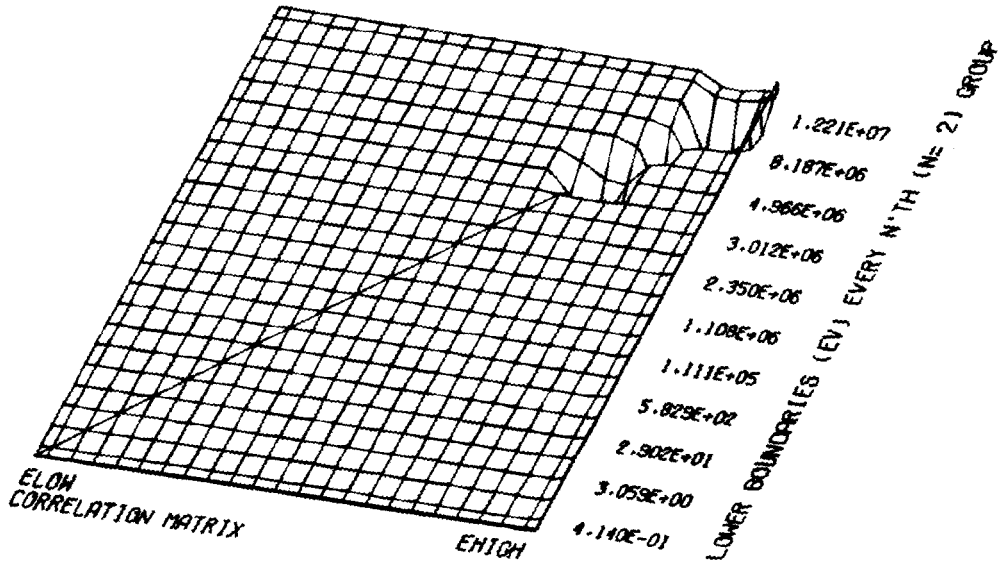

Fig. C-33. Correlation Matrix for Oxygen Elastic Cross Section as It Relates to the O(n,α) Cross Section.

ORNL DWG 75-6826

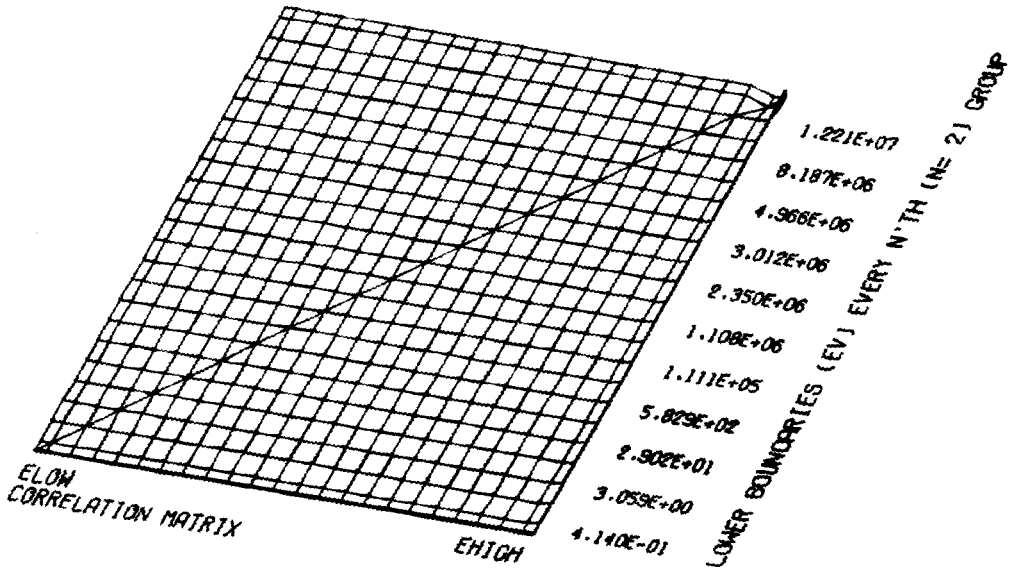

Fig. C-34. Correlation Matrix for Oxygen Inelastic Cross Section as It Relates to the O(n,p) Cross Section.

ORNL DWG 75-6827

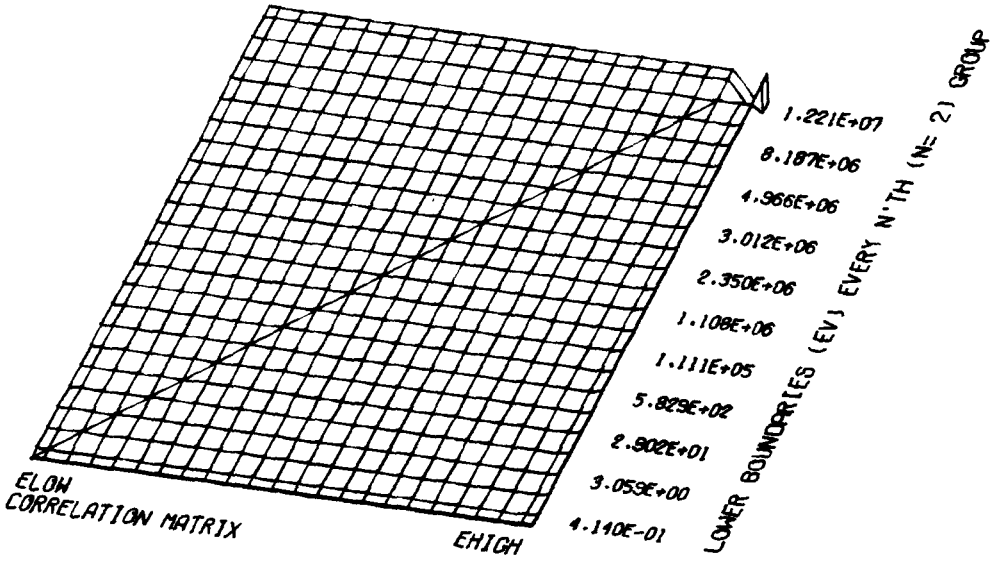

Fig. C-35. Correlation Matrix for Oxygen Inelastic Cross Section as It Relates to the O(n,α) Cross Section.

ORNL DWG 75-6828

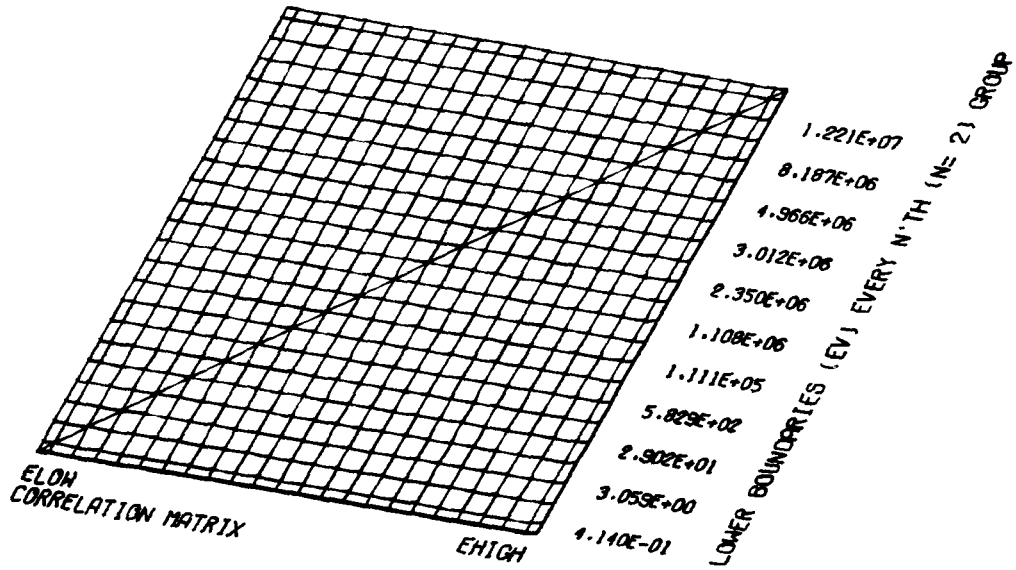

Fig. C-36. Correlation Matrix for O(n,p) Cross Section as It Relates to the O(n,α) Cross Section.

ORNL-TM-4847
(ENDF-218)

Internal Distribution

1-3. L. S. Abbott
4. R. G. Alsmiller, Jr.
5. J. Barish
6. D. E. Bartine
7. J. O. Blomeke
8. T. J. Burns
9. G. P. Cavanaugh
10. R. L. Childs
11. C. E. Clifford
12. S. N. Cramer
13. A. Croff
14. G. deSaussure
15. J. K. Dickens
16. F. C. Difillipo
17. J. D. Drischler
18. M. B. Emmett
19. W. W. Engle, Jr.
20. D. E. Ferguson
21. G. F. Flanagan
22. W. E. Ford
23. C. Y. Fu
24. T. A. Gabriel
25. N. M. Greene
26. R. Gwin
27. W. O. Harms
28. C. W. Kee
29. J. R. Knight
30. D. C. Larson
31. J. L. Lucius
32. R. E. Maerker
33. F. C. Maienschein
34. J. H. Marable
35. B. F. Maskewitz
36. G. W. Morrison
37-40. F. R. Mynatt
41. J. P. Nichols
42-44. E. M. Oblow
45. J. V. Pace
46. R. W. Peelle
47. F. G. Perey
48. R. B. Perez
49. L. M. Petrie
50. W. A. Rhoades
51. R. W. Roussin
52. R. T. Santoro
53. D. Steiner
54. P. N. Stevens
55. D. B. Trauger
56. D. K. Trubey
57-72. C. R. Weisbin
73. L. W. Weston
74. J. E. White
75. G. E. Whitesides
76. J. B. Wright
77. R. Q. Wright
78. P. F. Fox (consultant)
79. A. Henry (consultant)
80. W. W. Havens, Jr. (consultant)
81-82. Central Research Library
83-84. ORNL Y-12 Technical Library
85. Document Reference Section
86-89. Laboratory Records Department
90. Laboratory Records ORNL RC
91. ORNL Patent Office

External Distribution

92. A. M. Perry, Institute for Energy Analysis (ORAU), Oak Ridge, TN.
93. E. G. Silver, Institute for Energy Analysis (ORAU), Oak Ridge, TN.
94. M. Salvatores, Laboratorio Fisica Calcolo Reattore, C.S.N. Casaccia CNEN, Sp. Prob. Anguillarese Km+300, 00060 Rome, Italy
95. R. Oehlberg, Division of Reactor Safety Research, Energy Research and Development Administration, Washington, D. C. 20545
96. O. Ozer, Electric Power Research Institute, 3412 Hillview Avenue, P. O. Box 10412, Palo Alto, California 94304
97. J. W. Lewellen, Division of Reactor Research and Development, Energy Research and Development Administration, Washington, D. C. 20545

98. H. Henryson, II, Argonne National Laboratory, Applied Physics Division, 9700 South Cass Avenue, Argonne, Illinois 60439
99. D. R. Harris, Los Alamos Scientific Laboratory, Group T-2, Los Alamos, New Mexico 87544
100. R. Hunter, Los Alamos Scientific Laboratory, Group T-2, Los Alamos, New Mexico 87544
101. H. Motz, Los Alamos Scientific Laboratory, P Division Leader, Los Alamos, New Mexico 87544
102. D. Dudziak, Los Alamos Scientific Laboratory, Group T-1, Los Alamos, New Mexico 87544
103. K. Lathrop, Los Alamos Scientific Laboratory, Group T-1, Los Alamos, New Mexico 87544
104. R. J. LaBauve, Los Alamos Scientific Laboratory, Group T-2, Los Alamos, New Mexico 87544
105. W. E. Preeg, Los Alamos Scientific Laboratory, Group T-3, Los Alamos, New Mexico 87544
106. T. J. Hirons, Los Alamos Scientific Laboratory, Group T-6, Los Alamos, New Mexico 87544
107. T. England, Los Alamos Scientific Laboratory, Group T-2, Los Alamos, New Mexico 87544
108. J. J. Dorning, 214 Nuclear Engineering Laboratory, University of Illinois, Urbana, Illinois 61801
109. U. Farinilli, CNEN, Centro Di Studi Nucleari Della Casaccia, 00060-S, Maria Di Galleria, Rome, Italy
110. H. Gruppelaer, Stichting Reactor Centrum Nederland, Petten, Netherlands
111. J. J. Schmidt, IAEA, Nuclear Data Section, Kaerntner Ring 11-13, Vienna, Austria
112. L. J. Lidofsky, Columbia University, New York, New York 10027
113. R. Howerton, Lawrence Livermore Laboratory, Livermore, California 94550
114. G. L. Rogosa, Nuclear Science, Division of Physical Research, J-309, NRC, Washington, D. C. 20545
115. E. A. Straker, Science Applications, Inc., Huntsville, Alabama 35805
116. T. Albert, Science Applications, Inc., Huntsville, Alabama 35805
117. Norman Banks, U. S. Army Ballistics Research Laboratory, Aberdeen Proving Ground, MD 21005
118. A. R. Buhl, Division of Reactor Research and Development, Energy Research and Development Administration, Washington, D. C. 20545
119. R. Conn, University of Wisconsin, Nuclear Engineering Department, 1500 Johnson Drive, Madison, Wisconsin 53706
120. D. E. Cullen, Lawrence Livermore Laboratory, Livermore, California 94550
121. G. Foster, Los Alamos Scientific Laboratory, P. O. Box 1663, Los Alamos, New Mexico 87544
122. N. C. Francis, Knolls Atomic Power Laboratory, General Electric, P. O. Box 1072, Schenectady, New York 12301
123. S. A. W. Gerstl, Argonne National Laboratory, 9700 South Cass Avenue, Argonne, Illinois 60439

124. H. Goldstein, Columbia University, 287A Mudd Building, New York, New York 10027
125. P. Greebler, General Electric Company, Breeder Reactor Development Operation, 310 DeGuigne Drive, Sunnyvale, California 94086
126. E. Greenspan, Nuclear Research Center-Negev, P.O.B. 9001, Beer-Sheva 84190, Israel
127. G. Hale, Los Alamos Scientific Laboratory, P. O. Box 1663, Los Alamos, New Mexico 87544
128. J. P. Hamric, Division of Reactor Development and Technology, Energy Research and Development Administration, Washington, D. C. 20545
129. W. H. Hannum, Division of Reactor Research and Development, Energy Research and Development Administration, Washington, D. C. 20545
130. P. B. Hemmig, Division of Reactor Research and Development, Energy Research and Development Administration, Washington, D. C. 20545
131. T. J. Hoffman, Science Applications, Inc., Huntsville, Alabama 35805
132. V. A. Kamath, Scientific Advisor, ATTN: P. K. Patwardhan, Bhabha Atomic Research Centre, Trombay, Bombay, India
133. E. E. Kintner, Division of Reactor Research and Development, Energy Research and Development Administration, Washington, D. C. 20545
134. B. J. McGregor, Physics Division, A.A.E.C. - Res. Esta., Lucas Heights, Sidney, Australia
135. D. Muir, Los Alamos Scientific Laboratory, P. O. Box 1663, Los Alamos, New Mexico 87544
136. R. J. Neuhold, Division of Reactor Research and Development, Energy Research and Development Administration, Washington, D. C. 20545
137. P. F. Pasqua, Department of Nuclear Engineering, University of Tennessee, Knoxville, Tennessee
138. W. G. Price, Plasma Physics Laboratory, Princeton University, Princeton, New Jersey 08540
139. D. R. Riley, Division of Reactor Research and Development, Energy Research and Development Administration, Washington, D. C. 20545
140. J. N. Rogers, Division 8321, Sandia Laboratories, P. O. Box 969, Livermore, California 94550
141. M. E. Rose, Mathematical and Computer Sciences Program, Division of Physical Research, Energy Research and Development Administration, Washington, D. C. 20545
142. W. M. Stacey, Jr., Applied Physics Division, Argonne National Laboratory, 9700 South Cass Avenue, Argonne, Illinois 60439
143. Leona Stewart, Los Alamos Scientific Laboratory, P. O. Box 1663, Los Alamos, New Mexico 87544
144. Phil Young, Los Alamos Scientific Laboratory, P. O. Box 1663, Los Alamos, New Mexico 87544
145. J. Ching, Energy, Inc., Idaho Falls, Idaho

146. Luis Garcia de Viedma, Head of NEA, Computer Programme Library, Casella Postele N° 15, I 21027 - Ispra (VA) ITALY
147-272. National Neutron Cross Section Center, Brookhaven National Laboratory, Upton, New York
273-407. Given DNA Radiation Transport Distribution (updated 10-25-74)
408-409. Technical Information Center, ORO
410. Research and Technical Support Division, ERDA, ORO